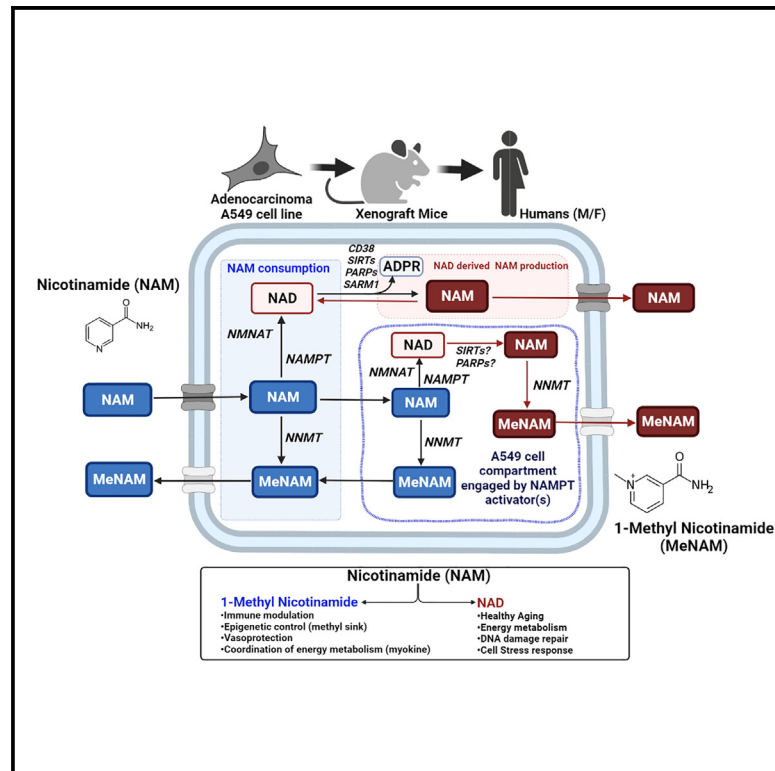


# Source of nicotinamide governs its metabolic fate in cultured cells, mice, and humans

## Graphical abstract



## Authors

Tumpa Dutta, Nidhi Kapoor, Meril Mathew, ..., Paul M. Coen, Gina M. DeNicola, Stephen J. Gardell

## Correspondence

tumpa.dutta@adventhealth.com (T.D.), stephen.gardell@adventhealth.com (S.J.G.)

## In brief

NAD<sup>+</sup> and 1-methylnicotinamide (MeNAM), which are produced from nicotinamide (NAM), differentially affect human health and aging. Metabolite tracing with <sup>2</sup>H<sub>4</sub>-NAM unveiled the metabolic fates of exogenous NAM and NAD<sup>+</sup>-derived NAM in cultured cells, mice, and humans. Exogenous NAM produced NAD<sup>+</sup> and MeNAM. NAD<sup>+</sup>-derived NAM was a poor precursor for MeNAM.

## Highlights

- Exogenous nicotinamide (NAM) produced NAD<sup>+</sup> and 1-methylnicotinamide (MeNAM)
- NAD<sup>+</sup>-derived NAM is a poor precursor for MeNAM
- Pioneering tracer study with <sup>2</sup>H<sub>4</sub>-NAM in humans
- NAMPT activators reprogram the metabolic fate of NAD<sup>+</sup>-derived NAM



## Article

# Source of nicotinamide governs its metabolic fate in cultured cells, mice, and humans

Tumpa Dutta,<sup>1,\*</sup> Nidhi Kapoor,<sup>1</sup> Meril Mathew,<sup>1</sup> Suban S. Chakraborty,<sup>1</sup> Nathan P. Ward,<sup>2</sup> Nicolas Prieto-Farigua,<sup>2</sup> Aimee Falzone,<sup>2</sup> James P. DeLany,<sup>1</sup> Steven R. Smith,<sup>1</sup> Paul M. Coen,<sup>1</sup> Gina M. DeNicola,<sup>2</sup> and Stephen J. Gardell<sup>1,3,\*</sup>

<sup>1</sup>Translational Research Institute, AdventHealth Orlando, Orlando, FL 32804, USA

<sup>2</sup>Department of Cancer Physiology, H. Lee Moffitt Cancer Center and Research Institute, Tampa, FL 33612, USA

<sup>3</sup>Lead contact

\*Correspondence: [tumpa.dutta@adventhealth.com](mailto:tumpa.dutta@adventhealth.com) (T.D.), [stephen.gardell@adventhealth.com](mailto:stephen.gardell@adventhealth.com) (S.J.G.)

<https://doi.org/10.1016/j.celrep.2023.112218>

## SUMMARY

Metabolic routing of nicotinamide (NAM) to NAD<sup>+</sup> or 1-methylnicotinamide (MeNAM) has impacts on human health and aging. NAM is imported by cells or liberated from NAD<sup>+</sup>. The fate of <sup>2</sup>H<sub>4</sub>-NAM in cultured cells, mice, and humans was determined by stable isotope tracing. <sup>2</sup>H<sub>4</sub>-NAM is an NAD<sup>+</sup> precursor via the salvage pathway in cultured A549 cells and human PBMCs and in A549 cell xenografts and PBMCs from <sup>2</sup>H<sub>4</sub>-NAM-dosed mice and humans, respectively. <sup>2</sup>H<sub>4</sub>-NAM is a MeNAM precursor in A549 cell cultures and xenografts, but not isolated PBMCs. NAM released from NAD<sup>+</sup> is a poor MeNAM precursor. Additional A549 cell tracer studies yielded further mechanistic insight. NAMPT activators promote NAD<sup>+</sup> synthesis and consumption. Surprisingly, NAM liberated from NAD<sup>+</sup> in NAMPT activator-treated A549 cells is also routed toward MeNAM production. Metabolic fate mapping of the dual NAM sources across the translational spectrum (cells, mice, humans) illuminates a key regulatory node governing NAD<sup>+</sup> and MeNAM synthesis.

## INTRODUCTION

Nicotinamide (NAM) is the amide form of vitamin B3 (niacin). Severe vitamin B3 deficiency causes pellagra, a systemic disease exhibiting the signature “4 Ds”: diarrhea, dermatitis, dementia, and, ultimately, death. Using NAM as a dietary supplement to prevent and treat pellagra was a monumental public health advance. Seminal research discoveries have unveiled why NAM is important for health. NAM is a precursor for NAD<sup>+</sup> synthesis via the NAD<sup>+</sup> salvage pathway. NAD<sup>+</sup> is an essential cofactor for redox enzymes playing indispensable roles in intermediary metabolism.<sup>1</sup> NAD<sup>+</sup> is also a substrate for poly(adenosine diphosphate-ribose) polymerases (PARPs), sirtuins, CD38, and sterile alpha and toll/interleukin-1 motif-containing 1 (SARM1).<sup>2</sup> The diverse actions of NAD<sup>+</sup>-consuming enzymes extend the biological impact of NAD<sup>+</sup> to a wide variety of crucial processes, including gene expression, DNA repair, epigenetics, cell signaling, and axon degeneration.

Another cellular fate for NAM is conversion to 1-methylnicotinamide (MeNAM) by NAM N-methyltransferase (NNMT) in the presence of S-adenosylmethionine (SAM), the universal methyl donor. NNMT is expressed in most tissues, including liver, adipose tissue, and skeletal muscle,<sup>3</sup> in addition to numerous human cancers.<sup>4</sup> In certain cell types, MeNAM is converted to methyl pyridone carboxamide derivatives (Me2PY, Me4PY, and Me6PY) by aldehyde oxidase (AOX).<sup>5,6</sup>

Emerging data show that MeNAM formation is more than simply a route for NAM clearance.<sup>7</sup> MeNAM was claimed to mediate cardiovascular benefits due to its putative vasoprotective, anti-

inflammatory, and anti-thrombotic effects.<sup>8</sup> MeNAM was also reported to be a novel myokine that enhanced utilization of energy stores in response to low muscle energy availability.<sup>9</sup> On the other hand, an inverse association between insulin sensitivity and plasma concentration of MeNAM was seen in patients with type 2 diabetes.<sup>10</sup> MeNAM was shown to be an immunoregulatory metabolite in human ovarian cancer that enhanced TNF- $\alpha$  expression and inhibited IFN- $\gamma$  production in T cells.<sup>11</sup> A mechanistic driver for certain biological effects of MeNAM involves its ability to serve as a methyl sink producing cellular epigenetic and transcriptional changes.<sup>4</sup> This collateral effect of MeNAM formation was shown to regulate cancer-associated fibroblast differentiation and cancer progression<sup>12</sup> as well as intrahepatic cholangiocarcinoma proliferation and metastasis.<sup>13</sup> The growing list of pivotal biological effects attributed to MeNAM makes it imperative to understand the molecular mechanisms governing its production.

Dietary NAM (i.e., exogenous NAM) is imported by cells via a putative plasma membrane carrier, which purportedly also transports MeNAM.<sup>14,15</sup> Another source of cell NAM is NAD<sup>+</sup> consumption mediated by PARPs, sirtuins, CD38, and SARM1. The metabolic fates of cellular NAM from the two sources, exogenous and NAD<sup>+</sup> derived, are not clearly defined. Whereas NAD<sup>+</sup>-derived NAM is salvaged to regenerate NAD<sup>+</sup>, the extents to which NAD<sup>+</sup>-derived NAM and imported NAM are used by NNMT to form MeNAM are unknown.

We used deuterated NAM (<sup>2</sup>H<sub>4</sub>-NAM) to trace the metabolic fates of exogenous NAM and NAM liberated from NAD<sup>+</sup> (Figure S1). Metabolite tracing was performed with cultured A549



lung adenocarcinoma cells.  $^2\text{H}_4$ -NAM was also administered intravenously (i.v.) to mice (A549 cell xenograft model) and humans followed by harvesting tumors/livers and peripheral blood mononuclear cells (PBMCs), respectively. Mass isotopomer distribution (MID) profiling of NAM and NAM-derived metabolites across the translational spectrum (cells, mice, and humans) revealed that the source of cell NAM (exogenous versus  $\text{NAD}^+$  derived) determined if NAM was a precursor for  $\text{NAD}^+$  or MeNAM. Additional  $^2\text{H}_4$ -NAM tracer studies in cultured A549 cells and isolated human PBMCs with tool compounds (NNMT inhibitor, CD38 inhibitor, nicotinamide phosphoribosyltransferase [NAMPT] activators; Figure S2) further illuminated mechanistic determinants governing the metabolic fate of NAM. Interestingly, our studies showed that NAMPT activators can reprogram NAM metabolism in A549 cells. Elucidating the alternative fates of NAM from the different sources is a crucial advance due to the disparate and impactful biological effects mediated by  $\text{NAD}^+$  and MeNAM.

## RESULTS

### Exogenous NAM is a precursor for both MeNAM and $\text{NAD}^+$ in cultured A549 cells

We first explored the metabolic fate of NAM in A549 cells by targeted metabolite profiling (Figure 1A). Conditioned medium (CM) from A549 cells grown for 18 h in medium containing 18  $\mu\text{M}$  NAM contained 14  $\mu\text{M}$  NAM (Figure 1B). The cellular NAM level in NAM-treated A549 cells was increased only 1.3-fold compared with A549 cells grown in NAM-free medium (Figure 1C). Hence, NAM in cell culture medium was consumed by A549 cells. Reduction of NAM in the medium was accompanied by a striking production of MeNAM in both cells (Figure 1D) and CM (Figure 1E). The elevated MeNAM level in CM,  $\sim 4 \mu\text{M}$ , mostly accounted for the loss of NAM. When A549 cells were grown in the presence of 18  $\mu\text{M}$  NAM, the cell levels of NAM and MeNAM (1.63 and 0.73 nmol/mg, respectively) were approximately 2-fold different. These data showed that cultured A549 cells contain NNMT activity, which briskly consumed NAM in the medium. NNMT was detected in A549 cell homogenates by western blotting using an anti-NNMT antibody (Figure S3A). In addition, NNMT activity was detected in A549 cell extracts but not A549 cell CM (Figure S3B).

Another metabolic fate for NAM in A549 cells is  $\text{NAD}^+$  formation via the salvage pathway. Addition of NAM to cell culture medium increased cell nicotinamide mononucleotide (NMN) (1.7-fold),  $\text{NAD}^+$  (1.9-fold), and NADH (1.9-fold) (Figures 1F–1H, respectively). NMN,  $\text{NAD}^+$ , and NADH levels in cells grown in the presence of NAM were 0.015, 6.1, and 0.14 nmol  $\text{mg}^{-1}$ , respectively. NAM-mediated elevations of NMN,  $\text{NAD}^+$ , and NADH were blocked by a NAMPT inhibitor (100 nM FK-866) (Figures 1F–1H). Conversely, a NAMPT activator (10  $\mu\text{M}$  SBI-797812)<sup>16</sup> increased the cellular NMN,  $\text{NAD}^+$ , and NADH levels in A549 cells by 8.7-, 1.9-, and 1.4-fold, respectively (Figures 1F–1H). Together, these data established that NAM was also utilized as a precursor for  $\text{NAD}^+$  synthesis in cultured A549 cells in a NAMPT-dependent manner.

Treatment of A549 cells with FK-866 slightly elevated the NAM level in the CM (12% increase) (Figure 1B). This result indicated

that  $\text{NAD}^+$  synthesis by A549 cells served as a sink for exogenous NAM. FK-866 treatment decreased cell NAM by 2.8-fold (Figure 1C). Accumulation of  $^2\text{H}_4$ -NAM by A549 cells was similar in the absence or presence of FK-866, which negated the possible impact of FK-866 on NAM uptake. Decreased cell NAM caused by FK-866 (Figures 1C and 1G) was linked to the accompanying decreased  $\text{NAD}^+$  level and the ability of  $\text{NAD}^+$  to serve as a source of cell NAM.

Neither FK-866 nor SBI-797812 changed the MeNAM level in A549 cells (Figure 1D) or CM (Figure 1E). Hence, altering the flow of NAM into the salvage pathway by manipulating NAMPT activity did not have an impact on MeNAM synthesis.

A small-molecule NNMT inhibitor (10  $\mu\text{M}$  NNMTi)<sup>17</sup> was used to probe the contribution of NNMT to NAM metabolism. NNMTi elicited huge decreases of MeNAM in both A549 cells and CM (79% and 80%, respectively) (Figures 1I and 1J). NAM levels in A549 cells and CM were increased slightly by NNMTi (Figures 1K and 1L). NNMTi treatment had no effect on the cellular  $\text{NAD}^+$  level in A549 cells (Figure 1M). Hence, surplus NAM from blocking MeNAM production was not rerouted to  $\text{NAD}^+$  synthesis.

### Stable isotope tracing with deuterated NAM ( $^2\text{H}_4$ -NAM) in A549 cells

A549 cells grown in 10  $\mu\text{M}$   $^2\text{H}_4$ -NAM (20  $\mu\text{M}$  total NAM) were assayed by liquid chromatography-mass spectrometry (LC-MS) for the MID profiles of NMN,  $\text{NAD}^+$ , NADH, NADP, NAM, and MeNAM (Figure 2A; Table S1).  $^2\text{H}_4$ -NAM was a major NMN precursor as seen by production of NMN(M4) (Figure 2B). Enrichment of NMN(M4) in the total NMN pool was 28%. Low amounts of NMN(M3) were also detected (6% enrichment).  $^2\text{H}_4$ -NAM treatment of cultured A549 cells also generated heavy-mass isotopomers for  $\text{NAD}^+$  (Figure 2C), NADH (Figure 2D), and NADP (Figure 2E). Enrichment values for  $\text{NAD}^+$ (M3) and  $\text{NAD}^+$ (M4) (26% and 6%, respectively), NADH(M3) and NADH(M4) (24% and 6%, respectively), and NADP(M3) and NADP(M4) (23% and 6%, respectively) were comparable. The preponderance of the M3- compared with the M4-mass isotopomers reflected removal of the C-4 deuterium by cell redox enzymes.<sup>18</sup> The similar MID profiles displayed by  $\text{NAD}^+$  and NADH reflected their rapid and extensive hydride ion interchange in A549 cells.

Treatment of A549 cells with  $^2\text{H}_4$ -NAM led to cellular accumulation of both NAM(M3) and NAM(M4) (Figure 2F). Enrichment values for cell NAM(M3) and NAM(M4) were 6% and 32%, respectively. NAM(M4) accumulation reflected cell uptake of  $^2\text{H}_4$ -NAM. Formation of NAM(M3) by  $^2\text{H}_4$ -NAM-treated A549 cells was a biomarker for consumption of  $\text{NAD}^+$  produced by the salvage pathway.<sup>19</sup> NAM(M3) is derived from  $^2\text{H}_4$ -NAM as follows: production of  $\text{NAD}^+$ (M4), conversion of  $\text{NAD}^+$ (M4) to  $\text{NAD}^+$ (M3) by cell oxidoreductases, and liberation of NAM(M3) by  $\text{NAD}^+$  glycohydrolases. NAM(M3) production signaled sequential  $\text{NAD}^+$  synthesis and degradation in cultured A549 cells. NAM(M3) also appeared in the CM of  $^2\text{H}_4$ -NAM-treated A549 cells (Figure 2G; Table S1). Enrichment of NAM(M3) in the NAM CM pool (1%) was dwarfed by high NAM (20  $\mu\text{M}$ ) in the medium.

A549 cells treated with  $^2\text{H}_4$ -NAM also produced abundant MeNAM(M4) (Figures 2H and 2I). Enrichment of MeNAM(M4) in the cell and CM MeNAM pools was 42% and 38%, respectively.

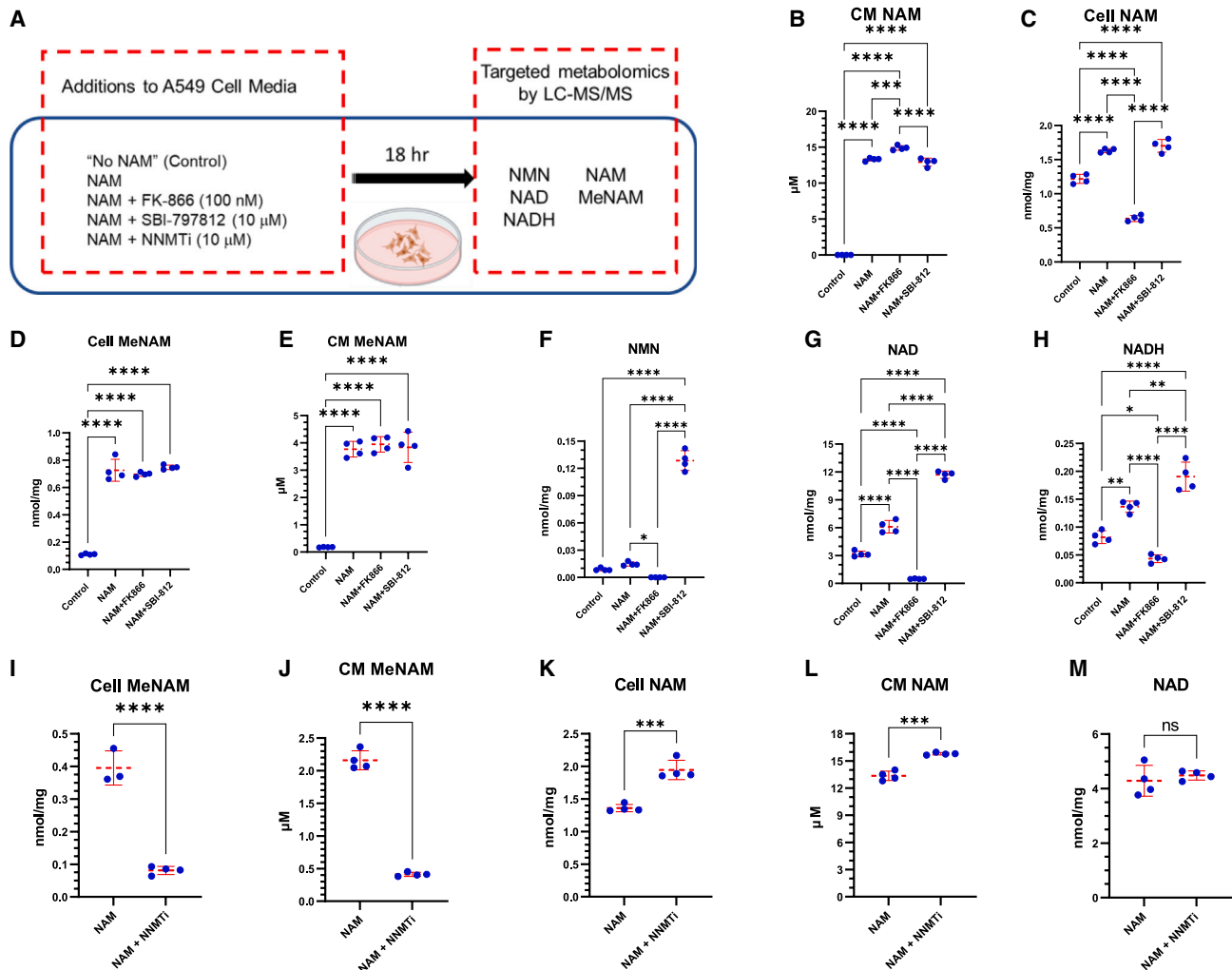


**Figure 1. Exogenous NAM has dual metabolic fates in cultured A549 cells**

(A) Experimental design. A549 cells were cultured in the absence (control) or presence of 18  $\mu\text{M}$  NAM plus 100 nM NAMPT inhibitor (FK-866), 10  $\mu\text{M}$  NAMPT activator (SBI-797812), or 10  $\mu\text{M}$  NNMT inhibitor (NNMTi). After 18 h, A549 cells and conditioned medium (CM) were harvested. Metabolites were assayed by LC-MS/MS.

(B–M) (B and L) CM NAM, (C and K) cell NAM, (D and I) cell MeNAM, (E and J) CM MeNAM, (F) cell NMN, (G and M) cell  $\text{NAD}^+$ , and (H) cell NADH. Metabolites in CM were reported as  $\mu\text{M}$ . Metabolites in cells were reported as  $\text{nmol mg}^{-1}$  protein. Data are represented as the mean  $\pm$  SD;  $n = 4$ . (B–H) Data were analyzed by one-way ANOVA multiple comparisons with Tukey's *post hoc* analysis; (I–M) data were analyzed by unpaired t test. ns, nonsignificant; \* $p < 0.05$ ; \*\* $p < 0.01$ ; \*\*\* $p < 0.001$ ; \*\*\*\* $p < 0.0001$ .

Hence, exogenous  $^2\text{H}_4$ -NAM was briskly metabolized by NNMT. Interestingly, the MeNAM(M3) level in  $^2\text{H}_4$ -NAM-treated A549 cells was very low (1% enrichment) (Figure 2H), despite the presence of appreciable cellular NAM(M3) (Figure 2F). This finding was the first clue that NAM derived from  $\text{NAD}^+$  consumption was a poor substrate for NNMT-mediated conversion to MeNAM.

#### Impact of NAMPT inhibition on the fate of $^2\text{H}_4$ -NAM in cultured A549 cells

Performing the  $^2\text{H}_4$ -NAM tracer study with FK-866 drastically reduced cellular NMN (Figure 2B).  $\text{NAD}^+$  and NADH were also decreased by 89% and 84%, respectively, by FK-866 versus

control cells (Figures 2C and 2D). M3 and M4 mass isotopomers for  $\text{NAD}^+$  or NADH were reduced to a greater extent in FK-866-treated cells. Results from this MID profiling study with  $^2\text{H}_4$ -NAM and FK-866 were consistent with the impressive NAMPT inhibitory effect of FK-866. Moreover, it further established the crucial role of the  $\text{NAD}^+$  salvage pathway for maintaining  $\text{NAD}^+$  and NADH levels in A549 cells.

NADP in FK-866-treated A549 cells was decreased by only 28% compared with control A549 cells (Figure 2E). However, FK-866 decreased NADP(M3) and NADP(M4) production to a much greater extent. These data showed that  $\text{NAD}^+$  was the precursor for NADP in A549 cells and the cellular turnover rate of NADP was more sluggish than that of  $\text{NAD}^+$  or NADH.

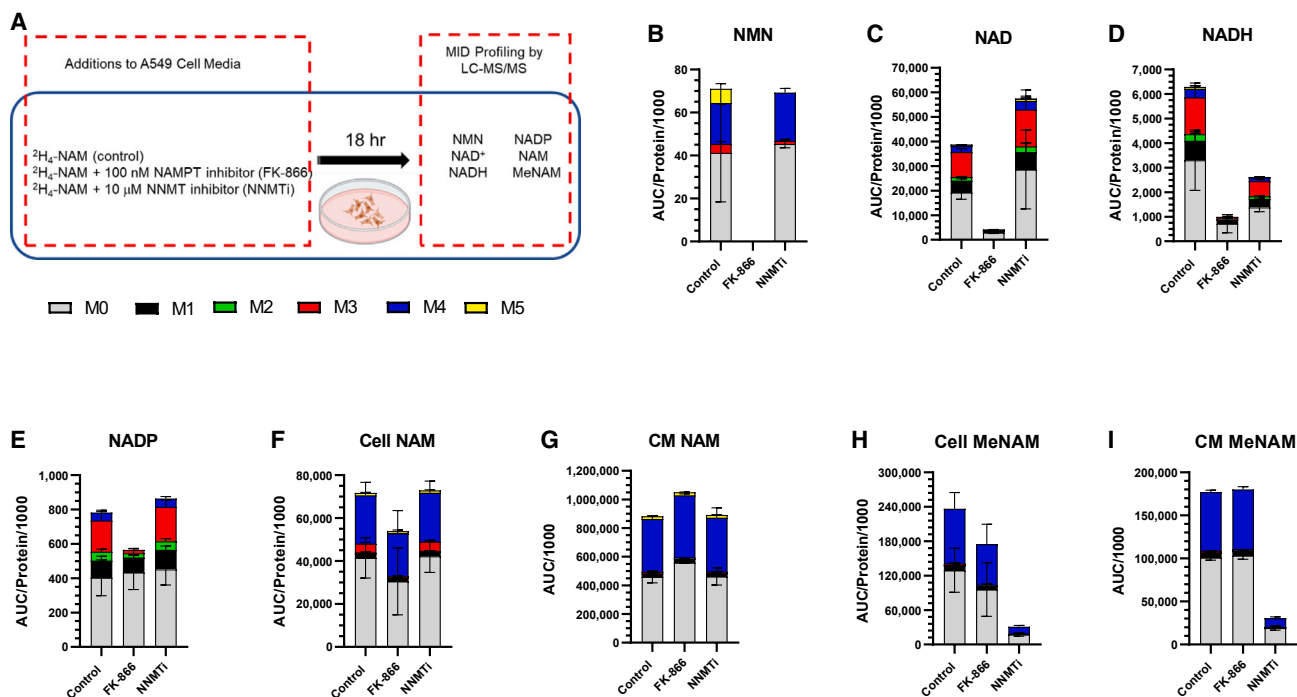


**Figure 2. Tracing NAM metabolism in A549 cells with  $^2\text{H}_4$ -NAM: Impact of inhibiting NAMPT and NNMT**

(A) Experimental design. A549 cells were cultured in  $20\ \mu\text{M}$  NAM ( $10\ \mu\text{M}$  NAM plus  $10\ \mu\text{M}$   $^2\text{H}_4$ -NAM) with and without  $100\ \text{nM}$  NAMPT inhibitor (FK-866) or  $10\ \mu\text{M}$  NNMT inhibitor (NNMTi) for 18 h.

(B–I) Cells and conditioned medium (CM) were analyzed by LC-MS for mass isotopomers (M0–M5; color coded) of (B) cell NMN, (C) cell  $\text{NAD}^+$ , (D) cell NADH, (E) cell NADP, (F) cell NAM, (G) CM NAM, (H) cell MeNAM, and (I) CM MeNAM. Cell AUC values were normalized to protein concentration and divided by 1,000. CM AUC values were divided by 1,000. Data are represented as the mean  $\pm$  SD for the mass isotopomers (M0–M5). See Table S1.

Treatment of A549 cells with FK-866 did not significantly affect the total cell NAM level (Figure 2F). However, FK-866 reduced NAM(M3) enrichment in A549 cells from 6% to 1%. These findings were consistent with sequential NAMPT-dependent production of NAD(M3) from  $^2\text{H}_4$ -NAM and its subsequent consumption to form NAM(M3).

FK-866 had little impact on the MID profiles for MeNAM in the  $^2\text{H}_4$ -NAM-treated A549 cells (Figure 2H) or CM (Figure 2I). Enrichment values for cell MeNAM(M4) in the absence and presence of FK-866 were 40% and 41%, respectively. Hence, blocking  $^2\text{H}_4$ -NAM utilization by the  $\text{NAD}^+$  salvage pathway did not re-route NAM to MeNAM formation. These data again pointed to the existence of disparate NAM pools in the A549 cells that differentially fueled  $\text{NAD}^+$  and MeNAM synthesis.

### Impact of NNMT inhibition on the fate of $^2\text{H}_4$ -NAM in cultured A549 cells

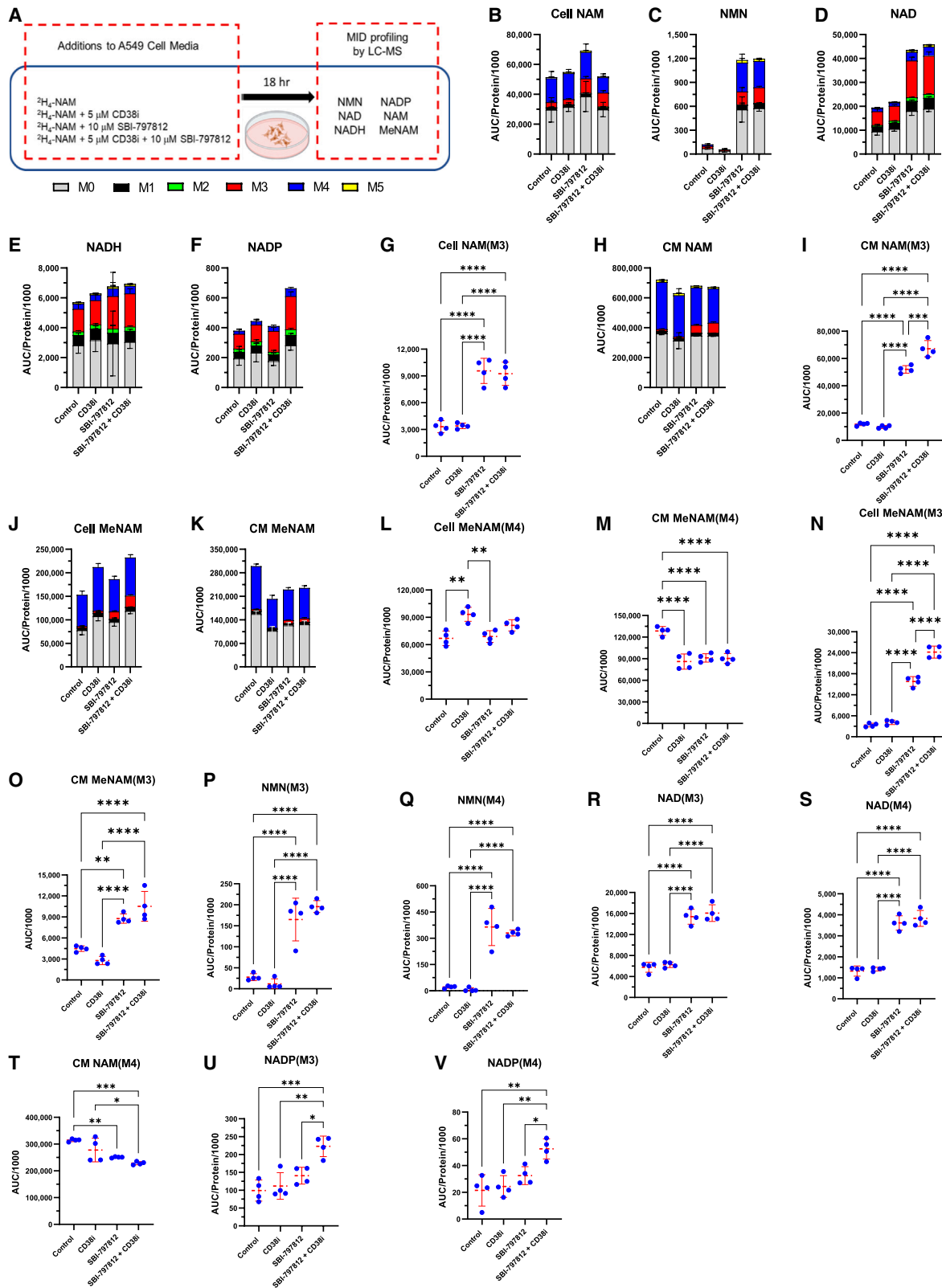
To further explore the role of NNMT in A549 cell NAM metabolism, we ran a  $^2\text{H}_4$ -NAM tracer study with NNMTi (Figure 2A; Table S1). Consistent with results from the targeted metabolite study (Figure 1), NNMTi dramatically reduced the MeNAM levels (area under the curve [AUC] sum of all mass isotopomers) in cells and CM by 87% and 83%, respectively (Figures 2H and 2I, respectively). Production of cell MeNAM(M3) and MeNAM(M4) was also blocked by NNMTi (89% and 87%, respectively). NNMTi did not change the levels or MID profiles of cellular

NMN (Figure 2B),  $\text{NAD}^+$  (Figure 2C), NADP (Figure 2E), or NAM (Figure 2F). There was a nonsignificant trend toward lower cell NADH due to NNMTi (Figure 2D). Importantly, this  $^2\text{H}_4$ -NAM tracer study confirmed that blocking the flow of NAM to MeNAM synthesis in A549 cells with NNMTi did not increase  $\text{NAD}^+$  production.

### Impact of CD38 inhibition on the fate of $^2\text{H}_4$ -NAM in A549 cells

$^2\text{H}_4$ -NAM tracer studies with A549 cells revealed substantial production of NAM(M3) from consumption of newly synthesized  $\text{NAD}^+$  (Figure 2F). Likely candidates mediating  $\text{NAD}^+$  degradation in A549 cells are sirtuins, PARPs, and CD38. CD38 is a  $\text{NAD}^+$ -glycohydrolase that consumes both NMN and  $\text{NAD}^+$ .<sup>20</sup> CD38 is expressed by A549 cells.<sup>21</sup> We probed the contribution of CD38 to  $\text{NAD}^+$  consumption in A549 cells and the fate of the liberated NAM using a CD38 inhibitor (CD38i)<sup>22</sup> (Figure 3A; Table S2).

Our initial attempt to assess the impact of CD38 on the metabolic fate of NAM in A549 cells showed that extracts prepared from CD38i-treated A549 cells had lower NAM levels compared with extracts from control cells. We concluded that CD38 was a major  $\text{NAD}^+$  consumer in A549 cells. A manuscript referee suggested that  $\text{NAD}^+$  degradation might occur during the post-experimental cell harvest. To explore this possibility, we revised our cell harvest protocol to include  $5\ \mu\text{M}$  CD38i in the cell wash



(legend on next page)

buffer. Blocking CD38 activity during the cell wash and harvest led to a 3-fold decrease in the cell NAM level (Figure S4). Hence, CD38 activity appeared to be latent in intact A549 cells but exposed during the cell wash step to produce NAM in the ensuing cell extract. This finding highlighted the importance of adding CD38i during the cell wash when performing metabolic tracer studies for NAD<sup>+</sup> synthesis and consumption in cultured cells. Cell tracer studies in the current article included CD38i during the cell wash step to avoid post-experimental NAD<sup>+</sup> consumption by CD38.

NAM levels in extracts prepared from A549 cells treated with and without CD38i were similar when CD38-mediated NAD<sup>+</sup> consumption was blocked during the cell harvest (Figure 3B). In addition, CD38i did not significantly impact the levels or MID profiles of NMN, NAD<sup>+</sup>, NADH, and NADP (Figures 3C–3F, respectively). These data revealed that CD38 in intact A549 cells was not an important regulator of NAD<sup>+</sup> synthesis or consumption. Notably, NAM(M3) was evident in A549 cells (6% enrichment) despite CD38i in the wash buffer (Figures 3B and 3G). NAM(M3) was also found in A549 cell CM (2% enrichment) at a level greater than its natural abundance (Figures 3H and 3I).

CD38i increased total MeNAM in A549 cells by 1.4-fold (Figure 3J) but decreased total MeNAM in the CM by 33% (Figure 3K). Likewise, CD38i increased MeNAM(M4) in A549 cells (Figure 3L) but decreased MeNAM(M4) in CM (Figure 3M). The opposing effects of CD38i on the MeNAM levels in A549 cells and CM were unexpected (Note: these findings were replicated in an independent experiment; see Figure S6). We performed an A549 cell tracer study with <sup>2</sup>H<sub>4</sub>-NAM to explore if CD38i blocked cell export of MeNAM. A549 cells were grown in <sup>2</sup>H<sub>4</sub>-NAM-containing medium and washed, and NAM-free medium was added with and without CD38i (Figure S5). Time-dependent loss of cellular MeNAM(M4) and appearance of CM MeNAM(M4) were both more sluggish in the presence of CD38i. Further studies are needed to clarify the mechanism for the apparent link between CD38 inhibition and impaired cell transport of MeNAM.

### Impact of NAMPT activators on the fate of <sup>2</sup>H<sub>4</sub>-NAM in cultured A549 cells

A <sup>2</sup>H<sub>4</sub>-NAM tracer study with A549 cells was performed with SBI-797812, a small-molecule NAMPT activator (Figure 3A; Table S2). As expected, SBI-797812 elevated cell NMN and NAD<sup>+</sup> by 10.7- and 2.2-fold, respectively (Figures 3C and 3D, respectively). Cell levels of the M3 and M4 mass isotopomers for NMN (Figures 3P and 3Q) and NAD<sup>+</sup> (Figures 3R and 3S) were also increased due to SBI-797812 treatment. Enrichment of NMN(M3) and NMN(M4) in cells treated with SBI-797812 was 14% and 31%, respectively. The corresponding enrichment values for the control cells were 25% and 19%, respectively. Hence, SBI-797812 slightly shifted the MID profile of NMN to-

ward NMN(M4) and away from NMN(M3). Enrichment values for NAD(M3) and NAD(M4) in the presence of SBI-797812 (35% and 8%, respectively) were like the enrichment values for the control cells (30% and 7%, respectively). SBI-797812 did not alter the levels or MID profiles of NADH (Figure 3E) or NADP (Figure 3F) in A549 cells.

SBI-797812 did not significantly change the cell NAM level (Figure 3B). However, SBI-797812 increased enrichment of NAM(M3) in the A549 cells (from 6% to 14%) and CM (from 2% to 8%) (Figures 3B and 3H). The levels of NAM(M3) in cells and CM were increased 2.9- and 4.4-fold, respectively, compared with control cells (Figures 3G and 3I). NAM(M3) accumulation in both A549 cells and CM due to SBI-797812 revealed that increased NAD<sup>+</sup> synthesis due to a NAMPT activator was accompanied by increased NAD<sup>+</sup> consumption. SBI-797812 also decreased NAM(M4) in CM, consistent with elevated NAD<sup>+</sup> biosynthetic flux via the salvage pathway (Figure 3T).

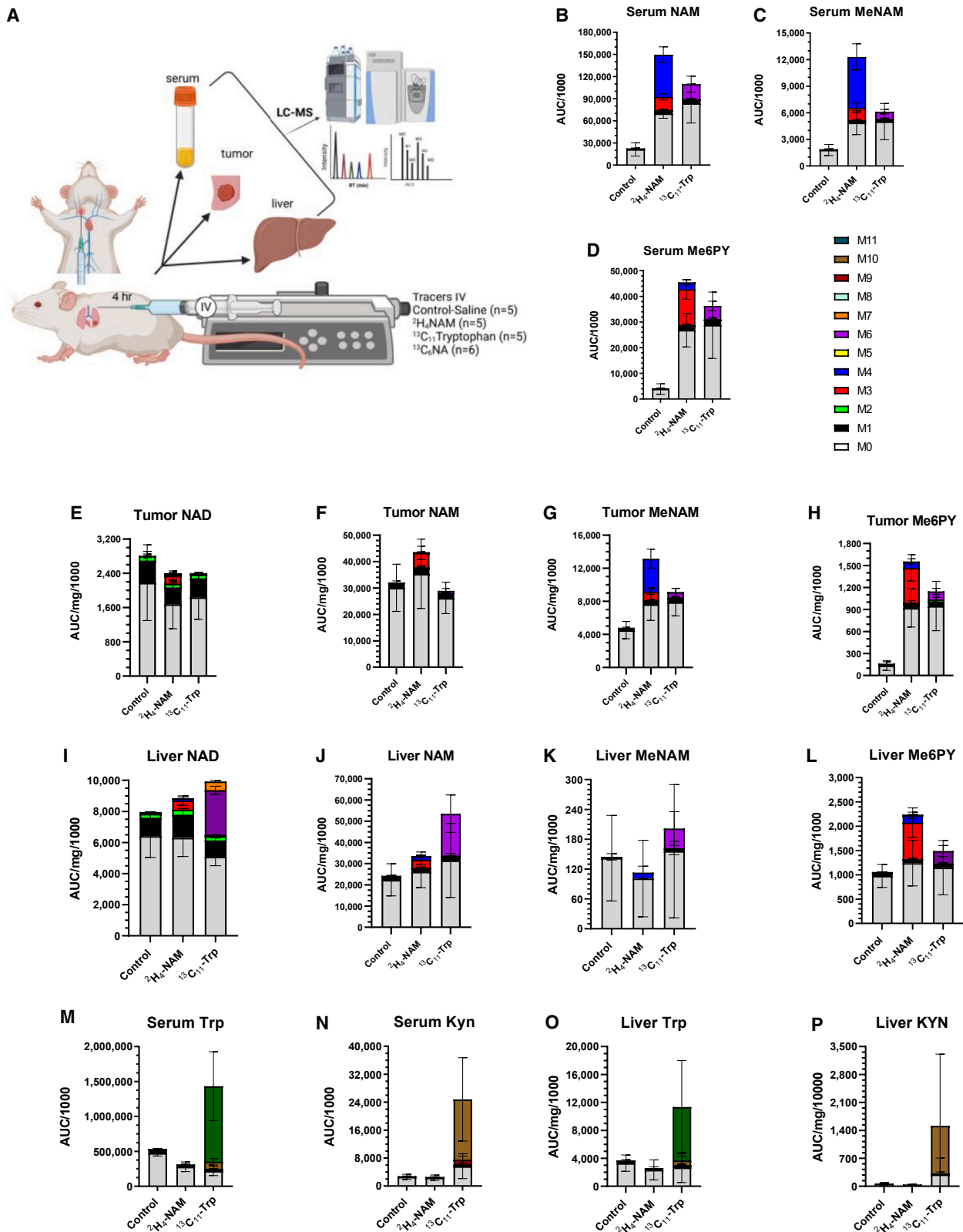
SBI-797812 did not significantly alter the cell level of total MeNAM (Figure 3J) or MeNAM(M4) (Figure 3L) but reduced the MeNAM(M4) level in CM by 29% (Figure 3M). Notably, SBI-797812 also increased the MeNAM(M3) level in A549 cells by 4.7-fold versus control cells (Figure 3N). There was an accompanying 2-fold increase in MeNAM(M3) in CM from SBI-797812-treated A549 cells (Figure 3O). This MeNAM(M3) data showed that NAD<sup>+</sup> produced in the presence of SBI-797812 yielded liberated NAM with greater propensity to serve as an NNMT substrate.

The distinctive ability of SBI-797812 to augment MeNAM(M3) production in A549 cells prompted us to examine if this effect was also seen with SBI-801071, a different NAMPT activator<sup>23</sup> (Figure S6A). We thus studied the impact of SBI-801071 on the metabolic fate of <sup>2</sup>H<sub>4</sub>-NAM in cultured A549 cells (Table S3). The effects of SBI-801071 on the levels and MID profiles for NMN and NAD<sup>+</sup> were comparable to those of SBI-797812 (Figures S6B–S6G). One difference between SBI-801071 and SBI-797812 was that the former raised the NADH level in A549 cells (Figures S6H–S6J) to a greater extent than the latter for unknown reasons. SBI-801071, like SBI-797812, did not have an impact on the abundance of or the MID profile for NADP (Figures S6K–S6M).

SBI-801071 increased cell production of NAM(M3) as evident by its accumulation in cells and CM (Figures S6N–S6R). This finding corroborated the results with SBI-797812 showing that the NAD<sup>+</sup> boosting effect of NAMPT activators was accompanied by increased NAD<sup>+</sup> consumption. The surprising finding that NAM(M3) produced in the presence of SBI-797812 was a better NNMT substrate was recapitulated with SBI-801071 (Figures S6S–S6X). Enrichment values for MeNAM(M3) for the control and SBI-801071-treated cells were 2% and 9%, respectively. The corresponding enrichment values for MeNAM(M3) in

### Figure 3. Tracing NAM metabolism in A549 cells with <sup>2</sup>H<sub>4</sub>-NAM: Impact of inhibiting CD38 and activating NAMPT

(A) Experimental design. A549 cells were cultured with <sup>2</sup>H<sub>4</sub>-NAM (10 μM NAM and 10 μM <sup>2</sup>H<sub>4</sub>-NAM) with and without 5 μM CD38i, 10 μM NAMPT activator (SBI-797812), or 5 μM CD38i plus 10 μM SBI-797812. Cells and conditioned medium (CM) were harvested after 18 h. (B–V) LC-MS was used for MID profiling of (B and G) cell NAM, (C, P, and Q) cell NMN, (D, R, and S) cell NAD, (E) cell NADH, (F, U, and V) cell NADP, (H, I, and T) CM NAM, (J, L, and N) cell MeNAM, and (K, M, and O) CM MeNAM. Cell AUC values were normalized to protein and divided by 1,000. CM AUC values were divided by 1,000. Color-coded key for B–F, H, J, K (M0–M5 mass isotopomers) is shown in (A). Data are represented as the mean ± SD for the mass isotopomers; See Table S2.



(legend on next page)

the CM were 1% and 4%, respectively. The ability of both SBI-797812 and SBI-801071 to promote MeNAM(M3) formation in A549 cells provides compelling evidence that NAMPT activators reprogrammed NAM metabolism.

### Probing possible interactions between CD38i and NAMPT activators in the metabolic fate of $^2\text{H}_4$ -NAM in A549 cells

The disparate  $\text{NAD}^+$  boosting mechanisms of NAMPT activators and CD38i prompted us to evaluate the impact of their combined treatment on the metabolic fate of  $^2\text{H}_4$ -NAM in A549 cells. Adding SBI-797812 and CD38i to A549 cells had no additional effect (compared with SBI-797812 alone) on NMN,  $\text{NAD}^+$ , or NADH (Figures 3C–3E, respectively). Combining CD38i with SBI-801071, instead of SBI-797812, had a similar outcome except that slightly decreased NMN(M4) and increased  $\text{NAD}^+$  were seen versus SBI-801071 alone (Figures S6D and S6E–S6G). Interestingly, the cell NADP level was increased by combining CD38i with either NAMPT activator, whereas these agents alone had no effect (Figures 3F, 3U, and 3V; Figures S6K–S6M).

Addition of CD38i along with SBI-797812 or SBI-801071 did not have an impact on the cell NAM(M3) level (Figures 3G and S6O). This finding supports our prior conclusion that CD38 was not a major  $\text{NAD}^+$  consumer in intact A549 cells. However, there were paradoxical increases in NAM(M3) in the CM when CD38i was combined with SBI-797812 (1.3-fold) or SBI-801071 (1.4-fold) (Figures 3I and S3R). The cell levels of MeNAM(M3) were also increased when CD38i was combined with SBI-797812 or SBI-801071 (Figures 3N and S6T). We attribute this effect to the purported ability of CD38i to block export of MeNAM from A549 cells as described above.

### Metabolic fate of $^2\text{H}_4$ -NAM in a murine A549 cell xenograft model

A murine A549 cell xenograft model was used to examine if the metabolic fate of NAM in cultured A549 cells was recapitulated *in vivo*. Mice with A549 cell xenografts were dosed (4 h. i.v. infusion) with vehicle control,  $^2\text{H}_4$ -NAM,  $^{13}\text{C}_{11}$ -Trp, or  $^{13}\text{C}_6$ -nicotinic acid ( $^{13}\text{C}_6$ -NA) (Figure 4A). Serum, tumors, and livers were interrogated by LC-MS to determine the metabolic fate of  $^2\text{H}_4$ -NAM (i.e., exogenous NAM) or NAM(M6) derived from  $^{13}\text{C}_{11}$ -Trp via sequential *de novo*  $\text{NAD}^+$  synthesis and  $\text{NAD}^+$  consumption (Tables S4–S6).

$^2\text{H}_4$ -NAM infusion increased total serum NAM by 6.6-fold (Figure 4B). Enrichment of NAM(M3) and NAM(M4) in the NAM serum pool was 12% and 38%, respectively. Appreciable NAM(M3) in serum from  $^2\text{H}_4$ -NAM-dosed mice revealed that sequential  $\text{NAD}^+$  synthesis from  $^2\text{H}_4$ -NAM and subsequent  $\text{NAD}^+$  consumption by  $\text{NAD}^+$  glycohydrolases occurred *in vivo*. The serum NAM(M0) level was increased 3.3-fold by the  $^2\text{H}_4$ -

NAM infusion (Figure 4B). This rise in serum NAM(M0), while not initially anticipated, was consistent with a prior study in which i.v. dosing of a different deuterated NAM derivative in rats raised the plasma NAM(M0) level.<sup>24</sup> Loading A549 cells with  $^2\text{H}_4$ -NAM (48 h treatment) followed by washing and medium replacement with 20  $\mu\text{M}$  NAM did not increase  $^2\text{H}_4$ -NAM in the CM, suggesting that the *in vivo* finding was not replicated in cultured cells.

The  $^2\text{H}_4$ -NAM infusion raised total serum MeNAM by 6.5-fold (Figure 4C). The total serum MeNAM AUC value was 8.2% of the total serum NAM AUC value. Enrichment of serum MeNAM(M3) and MeNAM(M4) was 11% and 47%, respectively. The serum enrichment values for the M3 and M4 mass isotopomers of MeNAM and NAM in  $^2\text{H}_4$ -NAM-dosed mice were comparable. The serum concentration of MeNAM(M0) was increased 2.7-fold due to the  $^2\text{H}_4$ -NAM infusion.

Me6PY, a metabolic product derived from MeNAM, was increased 8.7-fold in serum of  $^2\text{H}_4$ -NAM-infused mice (Figure 4D). Me6PY(M3), which is produced enzymatically from MeNAM(M4), was a prominent contributor to the elevated serum Me6PY level (31% enrichment). The serum Me6PY(M0) level was increased 6.9-fold by the  $^2\text{H}_4$ -NAM infusion.

We also explored the metabolic fate of  $^2\text{H}_4$ -NAM in A549 cell xenografts (Table S5). Total  $\text{NAD}^+$  levels were similar in tumors from vehicle control and  $^2\text{H}_4$ -NAM-dosed mice (Figure 4E). However,  $^2\text{H}_4$ -NAM was a precursor for tumor  $\text{NAD}^+$ , as evidenced by the appearance of NAM(M3) and NAM(M4) (7.7% and 1.9% enrichment, respectively). Total NAM trended higher in A549 cell tumors from  $^2\text{H}_4$ -NAM-treated mice versus vehicle-treated mice (Figure 4F). The tumor NAM pool contained NAM(M3) (12.5% enrichment) but there was little evidence of NAM(M4) (<1% enrichment). The low NAM(M4) likely reflected its highly efficient conversion to  $\text{NAD}^+$  or MeNAM. NAM(M3) in the A549 cell tumor revealed concomitant  $\text{NAD}^+$  synthesis and consumption. Notably, findings from the A549 cell xenografts of  $^2\text{H}_4$ -NAM-dosed mice were comparable to those obtained from cultured A549 cells treated with  $^2\text{H}_4$ -NAM.

Tumors from the murine xenograft model after the  $^2\text{H}_4$ -NAM infusion exhibited a 2.7-fold increase in total MeNAM compared with vehicle controls (Figure 4G). MeNAM(M4) in xenografts of  $^2\text{H}_4$ -NAM-dosed mice was nearly 4-fold more abundant than MeNAM(M3) (30% and 8% enrichment, respectively) despite the tumors containing higher levels of NAM(M3) compared with NAM(M4) (Figure 4B). MeNAM(M3) enrichment in A549 cell xenografts was 4-fold greater than in cultured A549 cells (compare Figures 4G, 2H, and 3J). One interpretation is that NAM(M3) released from NAM(M3) in the xenograft was a better NNMT substrate compared with NAM(M3) similarly produced in cultured A549 cells. However, another highly plausible explanation is that tumor MeNAM(M3) arose from the appreciable NAM(M3)

#### Figure 4. Tracing *in vivo* $\text{NAD}^+$ synthesis and consumption with $\text{NAD}^+$ precursors in a murine A549 cell xenograft model

(A) Experimental protocol.  $^2\text{H}_4$ -NAM,  $^{13}\text{C}_{11}$ -Trp, and  $^{13}\text{C}_6$ -nicotinic acid were i.v. infused in mice with A549 cell xenografts for 4 h followed by harvest of blood, xenografts, and liver.

(B–P) LC-MS was used for MID profiling of (B) serum NAM, (C) serum MeNAM, (D) serum Me6PY, (E) tumor  $\text{NAD}^+$ , (F) tumor NAM, (G) tumor MeNAM, (H) tumor Me6PY, (I) liver  $\text{NAD}^+$ , (J) liver NAM, (K) liver MeNAM, (L) liver Me6PY, (M) serum Trp, (N) serum Kyn, (O) liver Trp, and (P) liver Kyn. Serum AUC values were divided by 1,000. Tumor and liver AUC values were normalized to tissue mass (mg) and divided by 1,000. Data are represented as the mean  $\pm$  SD for the mass isotopomers (M0–M11). The color code key for the mass isotopomers is shown in (D). See Tables S4–S6.

in serum from  $^2\text{H}_4$ -NAM-infused mice (Figure 4B). NAM(M3) exported into blood from peripheral tissues of  $^2\text{H}_4$ -NAM-dosed mice will follow the same metabolic route as exogenous  $^2\text{H}_4$ -NAM, which includes serving as an NNMT substrate to form MeNAM(M3).

The Me6PY level in the xenografts was very low (Figure 4H). AUC values for total NAM, MeNAM, and Me6PY in xenografts from vehicle-infused mice (normalized to NAM) were 1.0, 0.15, and 0.005, respectively. However, xenograft Me6PY was increased 9.7-fold in  $^2\text{H}_4$ -NAM dosed mice versus vehicle controls. The expected mass isotopomer, Me6PY(M3), was a dominant contributor to the elevated tumor Me6PY pool (31% enrichment). We did not detect Me6PY in cultured A549 cells. The measurable level of Me6PY in the A549 cell xenografts might arise from metabolic pathway reprogramming of A549 cells in the tumor microenvironment, contributions from other cell types in the xenograft, or importation of Me6PY from the blood compartment.

Livers from  $^2\text{H}_4$ -NAM-infused mice were also interrogated for the MID profiles of  $\text{NAD}^+$ , NAM, MeNAM, and Me6PY (Figures 4I–4L). Vehicle control livers were unavailable. To assess fold changes in hepatic abundance due to infused  $^2\text{H}_4$ -NAM, livers from mice administered low-dose  $^{13}\text{C}_6$ -NA were used as a pseudo-control. Importantly, the  $^{13}\text{C}_6$ -NA infusion had no impact on the abundance or MID profiles of any of the measured metabolites in serum, tumor, or liver. Our use of livers from the  $^{13}\text{C}_6$ -NA-infused mice as the control group was further validated by the results of a prior murine tracer study using the same i.v. dose of  $^{13}\text{C}_6$ -NA, which also had no effect on the same set of metabolites.<sup>25</sup>

$\text{NAD}^+$  was not increased in murine liver due to the  $^2\text{H}_4$ -NAM infusion (Figure 4I). However, enrichment of NAD(M3) and NAD(M4) in the hepatic  $\text{NAD}^+$  pool (6.6% and 1.6%, respectively) showed that  $^2\text{H}_4$ -NAM was fueling the  $\text{NAD}^+$  salvage pathway in liver. The hepatic total NAM level trended slightly higher in  $^2\text{H}_4$ -NAM mice (1.4-fold) compared with control mice (Figure 4J). Enrichment of NAM(M3) and NAM(M4) was 12% and 5%, respectively, in livers from  $^2\text{H}_4$ -NAM-dosed mice. NAM(M3) in the liver revealed consumption of NAD(M3) by hepatic  $\text{NAD}^+$  glycohydrolases.

The hepatic MeNAM level was very low and unchanged by  $^2\text{H}_4$ -NAM dosing (Figure 4K). Indeed, the AUC value for hepatic MeNAM was <1% of the accompanying hepatic NAM AUC value. MeNAM(M4) was seen in livers from  $^2\text{H}_4$ -NAM-dosed mice (11% enrichment) but MeNAM(M3) was not. NNMT is highly expressed in the liver (Figure S3). Low abundance of MeNAM in the liver might reflect its rapid excretion or conversion to Me6PY. The hepatic level of Me6PY was increased 2.1-fold compared with the pseudo-control in  $^2\text{H}_4$ -NAM-dosed mice (Figure 4L). A key contributor to the increased Me6PY was Me6PY(M3) (34% enrichment).

Results from the  $^2\text{H}_4$ -NAM infusion study with the murine A549 cell xenograft model revealed that the  $\text{NAD}^+$  salvage pathway was active in both the xenograft and the liver. Newly synthesized  $\text{NAD}^+$  derived from the salvage pathway in xenografts and liver was consumed to release NAM. Importantly,  $\text{NAD}^+$ -derived NAM was a poor substrate for NNMT in the xenograft and liver, as was the case for cultured A549 cells.

### Metabolic fate of NAM derived from *de novo*-synthesized $\text{NAD}^+$ in mice

The metabolic fate of NAM released from  $\text{NAD}^+$  was further probed by infusing  $^{13}\text{C}_{11}$ -Trp in the murine A549 cell xenograft model (Figure 4A). This experimental approach relied on NAD(M6) production from  $^{13}\text{C}_{11}$ -Trp via the *de novo*  $\text{NAD}^+$  synthesis pathway followed by NAD(M6) cleavage by  $\text{NAD}^+$  glycohydrolases to form NAM(M6).

The  $^{13}\text{C}_{11}$ -Trp infusion increased total serum Trp by 2.7-fold (Figure 4M; Table S4). Trp(M11) enrichment in the serum Trp pool was 76%. The level of serum Kyn, a *de novo*  $\text{NAD}^+$  synthesis pathway intermediate, was increased 8.8-fold due to the  $^{13}\text{C}_{11}$ -Trp infusion (Figure 4N). The expected Kyn mass isotopomer derived from  $^{13}\text{C}_{11}$ -Trp, Kyn(M10), dominated in serum (70% enrichment).

$^{13}\text{C}_{11}$ -Trp dosing increased the total serum MeNAM and Me6PY levels by 3.2-fold ( $p = 0.06$ ) and 6.9-fold, respectively (Figures 4C and 4D). The accompanying serum enrichment values for MeNAM(M6) (Figure 4C) and Me6PY(M6) (Figure 4D) were each 14%. Serum AUC values for NAM(M6), MeNAM(M6), and Me6PY(M6), when normalized to NAM(M6), were 1, 0.04, and 0.25, respectively. The serum levels of MeNAM(M0) and Me6PY(M0) were increased 2.8- and 7.4-fold, respectively, by the  $^{13}\text{C}_{11}$ -Trp infusion.

More than 90% of Trp in blood is metabolized by the liver.<sup>26</sup> Liver is the major site for *de novo*  $\text{NAD}^+$  synthesis, for which Trp is the initial precursor.<sup>25</sup> We thus interrogated livers of  $^{13}\text{C}_{11}$ -Trp-infused mice for the MID profiles of Trp, Kyn,  $\text{NAD}^+$ , NAM, MeNAM, and Me6PY (Table S6). Hepatic Trp in mice dosed with  $^{13}\text{C}_{11}$ -Trp was increased 3.1-fold (compared with control livers). Trp(M11) was the dominant contributor (67% enrichment) (Figure 4O).  $^{13}\text{C}_{11}$ -Trp dosing also increased hepatic Kyn by 23-fold (Figure 4P). Enrichment of Kyn(M10) in the hepatic Kyn pool was 79%. A trend toward increased hepatic  $\text{NAD}^+$  in  $^{13}\text{C}_{11}$ -Trp-infused mice (1.25-fold elevation) was evident (Figure 4I). However, NAD(M6) clearly accumulated in livers of mice dosed with  $^{13}\text{C}_{11}$ -Trp. Enrichment of NAD(M6) in the liver  $\text{NAD}$  pool was 29%. Abundant hepatic NAD(M6) in  $^{13}\text{C}_{11}$ -Trp-infused mice revealed robust operation of the *de novo*  $\text{NAD}^+$  synthetic pathway in murine liver, unlike A549 cell xenografts (Figure 4E).

NAM levels in liver and serum from  $^{13}\text{C}_{11}$ -Trp-infused mice were increased 2.2- and 4.8-fold, respectively (compared with controls) (Figures 4J and 4B). Enrichment of NAM(M6) in the liver and serum NAM pools was 37% and 19%, respectively. These data established that  $\text{NAD}^+$  synthesized in murine liver from  $^{13}\text{C}_{11}$ -Trp was consumed by hepatic  $\text{NAD}^+$  glycohydrolases to produce NAM(M6). A major contributor to elevated serum NAM after the  $^{13}\text{C}_{11}$ -Trp infusion was a 3.9-fold increase in NAM(M0).

Low levels of MeNAM (Figure 4K) and Me6PY (Figure 4L) were detected in mouse liver. Total AUC values (normalized to NAM) for hepatic NAM, MeNAM, and Me6PY in  $^{13}\text{C}_{11}$ -Trp-infused mice were 1, 0.006, and 0.04, respectively. The  $^{13}\text{C}_{11}$ -Trp infusion did not alter the hepatic MeNAM level, but formation of MeNAM(M6) was evident (20% enrichment) (Figure 4K). Likewise, there was no significant change in the hepatic Me6PY level from the  $^{13}\text{C}_{11}$ -Trp infusion, but Me6PY(M6) was detected (17% enrichment) (Figure 4L).

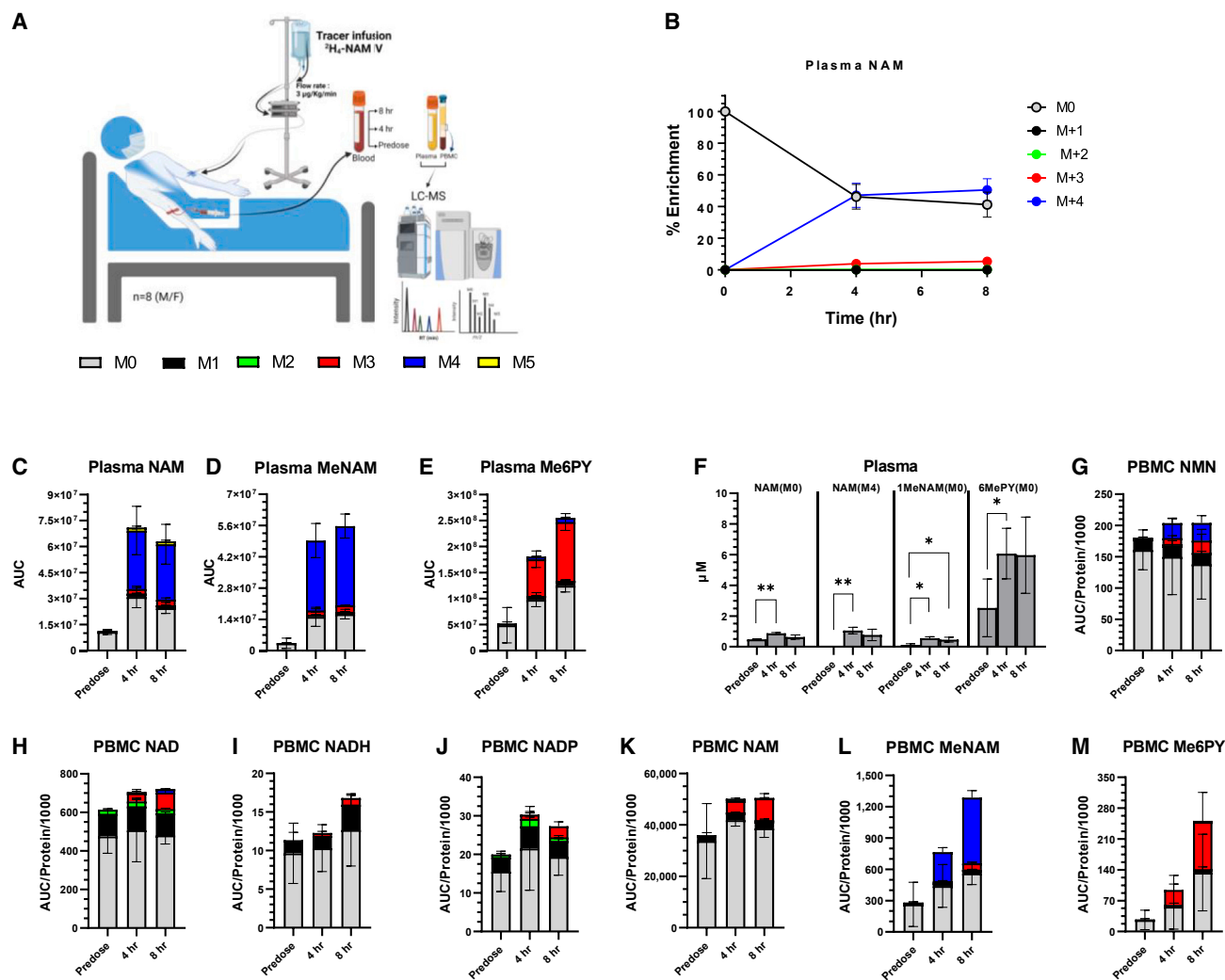


**Figure 5. Tracing *in vivo* NAM metabolism in humans with  $^2\text{H}_4$ -NAM**

(A) Experimental protocol.  $^2\text{H}_4$ -NAM was i.v. infused for 8 h in young adults. Blood was harvested for plasma and PBMCs at pre-dose, 4 h and 8 h. Data are shown for the high-dose  $^2\text{H}_4$ -NAM infusion ( $6.2 \mu\text{g kg}^{-1} \text{min}^{-1}$ ).

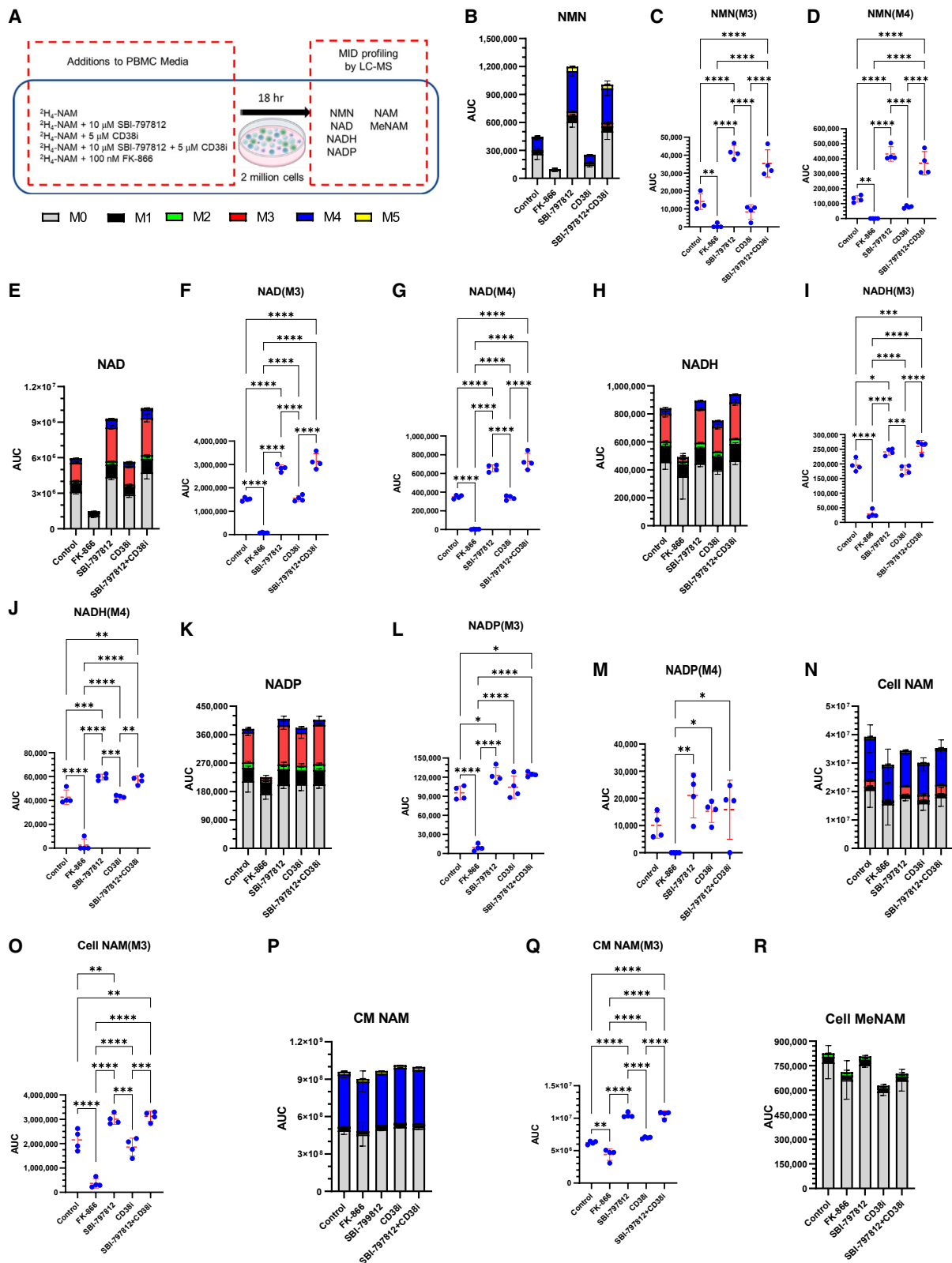
(B–M) (B–F) Plasma,  $n = 4$ . (G–M) PBMCs,  $n = 4$ . LC-MS was used for MID profiling of metabolites in plasma (B–E) and PBMCs (G–M). (B) Data reported as percentage enrichment. (C–E and G–M) Plasma and PBMC mass isotopomer levels reported as AUC values and AUC values normalized to cell protein ( $\times 10^{-3}$ ), respectively. (F) Plasma samples assayed by LC-MS/MS for the concentrations ( $\mu\text{M}$ ) of NAM(M0), NAM(M4), MeNAM(M0), and 6MePY(M0). (B and C) Plasma NAM, (D) plasma MeNAM, (E) plasma Me6PY, (G) PBMC NMN, (H) PBMC  $\text{NAD}^+$ , (I) PBMC NADH, (J) PBMC NADP, (K) PBMC NAM, (L) PBMC MeNAM, and (M) PBMC Me6PY. Data are represented as the mean  $\pm$  SD for the mass isotopomers; Data values (including the  $^2\text{H}_4$ -NAM low-dose group) and accompanying statistical analysis are provided in [Tables S8 and S9](#).

Only low levels of MeNAM(M6) and Me6PY(M6) were present in livers from mice dosed with  $^{13}\text{C}_{11}$ -Trp, despite appreciable hepatic NAM(M6). This suggested that  $\text{NAD}^+$ -derived NAM produced in the liver (i.e., NAM(M6)) was a poor NNMT substrate, as was the case for  $\text{NAD}^+$ -derived NAM in A549 cells, both in culture and when propagated as a xenograft. These low levels of MeNAM(M6) and Me6PY(M6) in livers from  $^{13}\text{C}_{11}$ -Trp-dosed mice need not arise from direct hepatic NNMT action on NAM(M6) liberated from hepatic  $\text{NAD}^+$ (M6). Substantial serum levels of NAM(M6) in  $^{13}\text{C}_{11}$ -Trp-dosed mice ([Figure 4B](#)) can supply an alternative indirect route for MeNAM(M6) and Me6PY(M6) formation in the liver. Accordingly, NAM(M6) can be secreted

and reabsorbed by the liver and processed akin to exogenous NAM rather than  $\text{NAD}^+$ -derived NAM.

### Metabolic fate of NAM in humans dosed intravenously with $^2\text{H}_4$ -NAM

Human volunteers were administered  $^2\text{H}_4$ -NAM to explore its metabolic fate ([Figure 5A](#)). Demographic data for the eight participants are provided in [Table S7](#). The first four and second four participants received  $1.49$  and  $2.91 \text{ mg kg}^{-1} \text{ } ^2\text{H}_4$ -NAM, respectively, via 8 h constant i.v. infusions. Blood was sampled before (baseline) and at 4 and 8 h after commencing the  $^2\text{H}_4$ -NAM infusion. Plasma was prepared from all eight subjects.



(legend on next page)

PBMCs were isolated from the four subjects who received high-dose  $^2\text{H}_4$ -NAM. MID profiling of NAM, MeNAM, and Me6PY in plasma and NMN, NAD<sup>+</sup>, NADP, NAM, MeNAM, and Me6PY in PBMCs was performed. Plasma and PBMC data are provided in Tables S8 and S9, respectively. Graphical data for the high-dose  $^2\text{H}_4$ -NAM group is presented (Figure 5).

Low- and high-dose  $^2\text{H}_4$ -NAM infusions in humans resulted in 37% and 51% enrichment of NAM(M4) in the plasma NAM pool, respectively, at 8 h (Figure 5B). Enrichment values for NAM(M4) were similar at the 4 and 8 h time points for both  $^2\text{H}_4$ -NAM-dose groups. NAM(M3) in plasma from  $^2\text{H}_4$ -NAM-infused subjects (5% enrichment at 8 h) (Figure 5C) revealed that  $^2\text{H}_4$ -NAM was incorporated into NAD<sup>+</sup>, which was subsequently degraded to liberate NAM. The  $^2\text{H}_4$ -NAM infusion also produced ample plasma MeNAM (Figure 5D). MeNAM(M4) was the dominant MeNAM mass isotopomer at 4 and 8 h. Small amounts of MeNAM(M3) were observed in plasma (5% enrichment).  $^2\text{H}_4$ -NAM was also a precursor for Me6PY in humans (Figure 5E). Me6PY(M3), the major Me6PY mass isotopomer in plasma produced from the  $^2\text{H}_4$ -NAM infusion, displayed enrichment values of 39% and 44% in the high-dose  $^2\text{H}_4$ -NAM group at 4 and 8 h, respectively.

As observed in the murine  $^2\text{H}_4$ -NAM and  $^{13}\text{C}_{11}$ -Trp tracer studies (Figure 4), plasma from  $^2\text{H}_4$ -NAM-dosed humans showed AUC elevations of the M0 mass isotopomers for NAM, MeNAM, and Me6PY (Figures 5C–5E). LC-MS/MS was used to precisely measure the plasma concentrations of NAM(M0), NAM(M4), MeNAM(M0), and Me6PY(M0) (Figure 5F). The pre-dose plasma levels of NAM(M0), MeNAM(M0), and Me6PY(M0) were 0.48, 0.12, and 2.5  $\mu\text{M}$ , respectively. The LC-MS/MS assays confirmed that the plasma levels of NAM(M0), MeNAM(M0), and Me6PY(M0) were increased by the  $^2\text{H}_4$ -NAM infusion. Plasma NAM(M0) was increased 1.8- and 1.3-fold at 4 and 8 h, respectively. Plasma MeNAM(M0) was increased 4.6- and 3.8-fold at 4 and 8 h, respectively. Finally, plasma Me6PY(M0) was increased 2.4-fold at both 4 and 8 h. Plasma levels of NAM(M0) and NAM(M4) after the high-dose  $^2\text{H}_4$ -NAM infusion were comparable.

Analysis of PBMCs from  $^2\text{H}_4$ -NAM-dosed humans revealed conspicuous NAM metabolism. NMN(M4) enrichment in the PBMC NMN pool of high-dose  $^2\text{H}_4$ -NAM participants was 15% (Table S9; Figure 5G). Enrichment of NMN(M4) in PBMCs was similar at both the 4 and the 8 h time points. In contrast, NMN(M3) enrichment was increased approximately 2-fold from 4 to 8 h (5% and 10%, respectively) (Figure 5G). NAD(M3) and NAD(M4) were also observed in PBMCs from  $^2\text{H}_4$ -NAM-dosed humans (Table S9; Figure 5H). The level of NAD(M3) in PBMCs was approximately 5-fold higher than that of NAD(M4). Enrichment of NAD(M3) in PBMCs was 7% and 14% at 4 and 8 h, respectively. Hence, there was an approximate 2-fold increased NAD<sup>+</sup> enrichment in PBMCs as the  $^2\text{H}_4$ -NAM infusion was prolonged from 4 to 8 h. There was also evidence for incorporation

of  $^2\text{H}_4$ -NAM into the NADH and NADP pools of PBMCs isolated from human volunteers (Figures 5I and 5J, respectively).

The  $^2\text{H}_4$ -NAM infusion in humans did not significantly increase NAM in PBMCs (Figure 5K). In addition, very little NAM(M4) was detected in the PBMCs (Figure 5K). We inferred that  $^2\text{H}_4$ -NAM imported by PBMCs is efficiently utilized to form NAD<sup>+</sup> (Figure 5H). However, time-dependent accumulation of NAM(M3) in PBMCs was observed. Enrichment of NAM(M3) was 9% and 17% at 4 and 8 h, respectively. Hence, NAM generated via NAD<sup>+</sup> consumption in PBMCs from humans dosed with  $^2\text{H}_4$ -NAM appeared to accumulate in PBMCs, unlike exogenous NAM.

MeNAM levels were very low in PBMCs isolated from  $^2\text{H}_4$ -NAM-infused humans but appeared to increase in a time-dependent manner (Figure 5L). Importantly, MeNAM(M4) greatly exceeded MeNAM(M3), despite the accompanying excess of NAM(M3) compared with NAM(M4) (Figure 5K). Enrichment of MeNAM(M4) in the PBMC fraction at 4 and 8 h was 39% and 50%, respectively. Me6PY in PBMCs from  $^2\text{H}_4$ -NAM-infused subjects was also very low but appeared to increase in a time-dependent manner (Figure 5M). Me6PY(M3) was the dominant heavy mass isotopomer of Me6PY.

#### Metabolic fate of NAM in isolated human PBMCs treated with $^2\text{H}_4$ -NAM

We performed a  $^2\text{H}_4$ -NAM tracer study with isolated human PBMCs to profile the metabolic fate of NAM in human cells other than transformed A549 cells (Figure 6A; Table S10). PBMCs treated with  $^2\text{H}_4$ -NAM produced M3 and M4 mass isotopomers of NMN, NAD<sup>+</sup>, NADH, and NADP (Figures 6B–6M). Enrichment values for cell M3 mass isotopomers of NMN, NAD<sup>+</sup>, NADH, and NADP were 3%, 25%, 23%, and 25%, respectively. The corresponding values for the M4 mass isotopomers were 29%, 6%, 5%, and 3%, respectively.

Human PBMCs treated with  $^2\text{H}_4$ -NAM contained appreciable NAM(M3) (5% enrichment) (Figures 6N and 6O). Enrichment of NAM(M3) in PBMCs was far lower than that of NAM(M4) (37%) (Figures 6N and 6P), reflecting the dominance of imported  $^2\text{H}_4$ -NAM. NAM(M3) was also detected in CM from  $^2\text{H}_4$ -NAM-treated PBMCs (Figures 6P and 6Q) but at a low enrichment (1%) due to plentiful NAM in the medium. Hence, MID results from PBMCs treated *in vitro* with  $^2\text{H}_4$ -NAM revealed both NAD<sup>+</sup> synthesis and NAD<sup>+</sup> consumption, which largely recapitulated tracer findings with A549 cells (grown both in culture and as a murine xenograft) and PBMCs isolated from  $^2\text{H}_4$ -NAM-dosed humans.

The MeNAM AUC value in PBMCs treated with  $^2\text{H}_4$ -NAM *in vitro* (Figure 6R) was 50-fold lower than the accompanying NAM AUC value (Figure 6N). Enrichment of MeNAM(M3) and MeNAM(M4) in the cell MeNAM pool was negligible (Figure 6R). MeNAM was undetectable in CM from the *in vitro* PBMC tracer experiment. This result ruled out that MeNAM was appreciably synthesized in  $^2\text{H}_4$ -NAM-treated PBMCs followed by rapid cell

#### Figure 6. *In vitro* $^2\text{H}_4$ -NAM tracing in human PBMCs

(A) Experimental design. Isolated human PBMCs ( $2.0 \times 10^6$  cells) were cultured in 20  $\mu\text{M}$  NAM (10  $\mu\text{M}$  NAM plus 10  $\mu\text{M}$   $^2\text{H}_4$ -NAM) with and without 100 nM FK-866, 10  $\mu\text{M}$  SBI-797812, 5  $\mu\text{M}$  CD38i, or 10  $\mu\text{M}$  SBI-797812 plus 5  $\mu\text{M}$  CD38i. Cells and conditioned medium (CM) were collected after 18 h. (B–R) LC-MS was used for MID profiling of (B–D) cell NMN, (E–G) cell NAD<sup>+</sup>, (H–J) cell NADH, (K–M) cell NADP, (N and O) cell NAM, (P and Q) CM NAM, and (R) cell MeNAM. AUC values are shown. Data represent the mean  $\pm$  SD, n = 4 for the mass isotopomers. Color code for (B), (E), (H), (K), (N), and (P) is depicted in (A). See Table S10.

export. Together, these findings revealed that the MeNAM synthesis arm of the bifurcated NAM metabolic fate pathway was inoperable in isolated human PBMCs. This conclusion is compatible with a recent report showing that PBMCs express very low levels of NNMT.<sup>11</sup>

Comparing MeNAM MID profiles of PBMCs treated *in vitro* with <sup>2</sup>H<sub>4</sub>-NAM (Figure 6R) with those of PBMCs from <sup>2</sup>H<sub>4</sub>-NAM-infused humans (Figure 5L) revealed an intriguing difference. MeNAM(M4) was not detected in the former but was conspicuous in the latter (49% enrichment). We hypothesized that MeNAM(M4) was produced in <sup>2</sup>H<sub>4</sub>-NAM-infused humans by peripheral tissues, exported into the blood, and imported into PBMCs. This scenario lends credence to MeNAM being an important signaling molecule rather than simply an elimination route for excess NAM.

The effects of tool compounds (FK-866, SBI-797812, CD38i) on the metabolic fate of <sup>2</sup>H<sub>4</sub>-NAM when added to isolated PBMCs were comparable to those seen with A549 cells. FK-866 markedly reduced the cell NMN and NAD<sup>+</sup> (Figures 6B–6G). Their M3 and M4 mass isotopomers were decreased by FK-866 to a much greater extent. This result is consistent with the remarkable ability of FK-866 to inhibit NAMPT. FK-866 had lesser effects on the cell levels of NADH and NADP (versus NMN and NAD<sup>+</sup>), but production of the corresponding M3 and M4 mass isotopomers was abolished (Figures 6H–6M). These findings revealed that turnover of NADH and NADP in PBMCs was slower than that of NMN and NAD<sup>+</sup>.

SBI-797812 increased NMN and NMN(M3) by 2.7- and 3.3-fold, respectively, in isolated PBMCs treated with <sup>2</sup>H<sub>4</sub>-NAM (Figures 6B and 6C). SBI-797812 also increased cellular total NAD<sup>+</sup>, NAD(M3), and NAD(M4) by 1.6-, 1.9-, and 1.9-fold, respectively (Figures 6E–6G). SBI-797812 did not raise cell NADH (Figures 6H–6J) or NADP (Figures 6K–6M), but modest increases in NADH(M3), NADH(M4), and NADP(M3) were seen. Apparent uncoupling of the ability of SBI-797812 to increase NAD<sup>+</sup> but not NADH or NADP, despite contemporaneous synthesis of all three pyridine nucleotides (deduced from the MID profiles), likely reflects cell homeostatic mechanisms that exert stricter control of the NADH and NADP levels.

Interestingly, SBI-797812 in the *in vitro* PBMC <sup>2</sup>H<sub>4</sub>-NAM tracer study increased NAM(M3) in CM by 1.7-fold (Figures 6P and 6Q). These data further established that the NAD<sup>+</sup> boosting effect of NAMPT activators was held in check by cell NAD<sup>+</sup> consumers.

CD38i did not significantly change the levels of NMN, NAD<sup>+</sup>, NADH, and NADP in <sup>2</sup>H<sub>4</sub>-NAM-treated PBMCs (Figures 6B–6M). Moreover, CD38i did not alter the levels of NAM(M3) in the cells or CM (Figures 6N–6Q). We concluded that, while CD38i is highly expressed by PBMCs,<sup>27</sup> it is not a key driver of constitutive NAD<sup>+</sup> consumption in resting PBMCs. Hence, NAD<sup>+</sup> glycohydrolases other than CD38i appear to mediate the observed NAD<sup>+</sup> consumption. Finally, results of combining CD38i with SBI-797812 in the *in vitro* PBMC <sup>2</sup>H<sub>4</sub>-NAM tracer study were no different than with SBI-797812 alone.

## DISCUSSION

NAM is a vital cellular nutrient that is imported by cells (i.e., exogenous NAM) or liberated from NAD<sup>+</sup> by NAD<sup>+</sup> consumers

(i.e., NAD<sup>+</sup>-derived NAM). These dual sources of cell NAM can have alternative metabolic fates. NAM is a precursor for NAD<sup>+</sup> or MeNAM via the salvage pathway or NNMT, respectively. Metabolic routing of NAM to NAD<sup>+</sup> or MeNAM has crucial biological implications. NAD<sup>+</sup> produced from NAM is a cofactor for cell oxidoreductases and a substrate for sirtuins, PARPs, CD38, and SARM1. MeNAM produced by NNMT in the presence of NAM and SAM mediates a different set of biological actions, including immune modulation, epigenetic control, vasoprotection, and coordination of cellular energy metabolism. Herein, we used stable isotope tracing to elucidate the metabolic fate of NAM in cultured A549 cells, mice, and humans. Importantly, we showed that the source of cell NAM governed its metabolic fate similarly across the translational spectrum.

Exogenous <sup>2</sup>H<sub>4</sub>-NAM was a precursor for both NAD<sup>+</sup> and MeNAM in cultured cells, mice, and humans (Figure 7). The dominant NAD<sup>+</sup> mass isotopomer derived from <sup>2</sup>H<sub>4</sub>-NAM was NAD(M3) instead of NAD(M4), due to ubiquitous oxidoreductases that convert NAD(M4) to NAD(M3). This is a fortuitous chemical transformation because NAD(M3) cleavage by cell NAD<sup>+</sup> glycohydrolases yields NAM(M3), which can be used to trace the fate of NAD<sup>+</sup>-derived NAM. Surprisingly, NAD<sup>+</sup>-derived NAM was exported from A549 cells and used to resynthesize NAD<sup>+</sup> but was a poor NNMT substrate. We emphasize that A549 xenografts/livers from mice dosed *i.v.* with <sup>2</sup>H<sub>4</sub>-NAM or <sup>13</sup>C<sub>11</sub>-Trp, as well as PBMCs from humans dosed *i.v.* with <sup>2</sup>H<sub>4</sub>-NAM, exhibited this same restricted metabolic fate for NAD<sup>+</sup>-derived NAM.

The appearance of NMN(M3) in the <sup>2</sup>H<sub>4</sub>-NAM tracer studies can arise from several cell routes. NAM(M3) liberated from NAD(M3) can be used as a precursor for NMN(M3) via the salvage pathway. Channeling of NAM(M3) to NMN(M3) synthesis or secretion is an important topic for future investigation. Other sources of NMN(M3) are possible, such as the reverse nicotinamide mononucleotide adenylyltransferase (NMNAT) reaction involving NAD(M3) and the use of NMN(M4) as a noncanonical redox cofactor.

Metabolic routing of NAM in A549 cells appeared to be reprogrammed by NAMPT activators. SBI-797812 and SBI-801071 increased <sup>2</sup>H<sub>4</sub>-NAM utilization via the salvage pathway as revealed by MID profiling of NMN and NAD<sup>+</sup>. Surprisingly, NAMPT activators also elicited increased production of MeNAM(M3) in A549 cells (Figure 7). NAMPT activators thus appear to promote NAD<sup>+</sup> synthesis in a putative cell compartment containing both NAMPT and NNMT. This contrasts with NAD<sup>+</sup> synthesis in A549 cells under control conditions when liberated NAM was not subject to NNMT action. Increased MeNAM(M3) by NAMPT activators was not suppressed by CD38 inhibition. Hence, an NAD<sup>+</sup> glycohydrolase other than CD38 cleaved NAD<sup>+</sup> in this “NAMPT activator-responsive” compartment in A549 cells to release NAM that was a substrate for NNMT.

NAD<sup>+</sup> metabolism and signaling are influenced by cell compartmentalization constraints.<sup>28,29</sup> We hypothesized that the disparate metabolic fates of exogenous NAM and NAD<sup>+</sup>-derived NAM arose from differential sequestration of NAM-generating and -consuming enzymes in the various subcellular compartments. The subcellular locales of NAM producers,

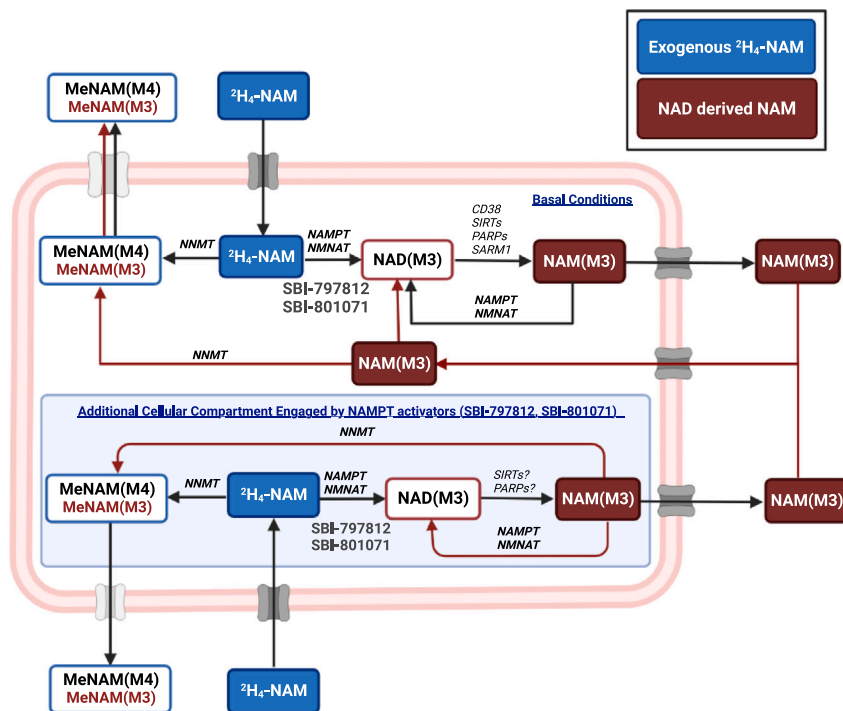


**Figure 7. NAM metabolism in A549 cells unveiled by  $^2\text{H}_4$ -NAM metabolic tracing**

$^2\text{H}_4$ -NAM (exogenous NAM) was imported by A549 cells and used as a precursor for NAD(M4) via the sequential actions of NAMPT and NMNAT. NAD(M4) was converted to NAD(M3) due to the cycling of  $\text{NAD}^+$  and NADH by cell redox enzymes.  $^2\text{H}_4$ -NAM was also an NNMT substrate giving rise to MeNAM(M4), which was exported from A549 cells. NAM(M3) was produced from NAD(M3) by the actions of one or more  $\text{NAD}^+$  consumers (sirtuin and PARP family members are likely mediators). NAM(M3) was exported from the cell or used by the salvage pathway to regenerate  $\text{NAD}^+$ . NAM(M3) was a poor NNMT substrate in A549 cells, as shown by low MeNAM(M3) in cells and CM. NAMPT activators, SBI-797812 and SBI-801071, increased enrichment of NAD(M3), consistent with their mechanism of action. Concomitant increase in NAM(M3) by NAMPT activators showed that the greater  $\text{NAD}^+$  synthetic flux was accompanied by higher  $\text{NAD}^+$  consumptive flux. Interestingly, the MeNAM(M3) level was increased in both cells and CM by NAMPT activators. The ability of NAMPT activators to promote MeNAM(M3) production was not blocked by CD38i. We hypothesized that a portion of the elevated NAD(M3) due to NAMPT activators occurred in a subcellular compartment where it was processed by an  $\text{NAD}^+$ -glycohydrolase (other than CD38) to give rise to NAM(M3) that was now accessible to NNMT action.

including sirtuins, PARPs, and CD38, are varied. As for NAM consumers, NNMT is a cytosolic enzyme, whereas NAMPT is localized in the nucleus and cytoplasm.<sup>30</sup> There is also evidence for regulated transport of NAMPT between cytosol and nucleus. Another ill-defined subcellular compartment for NAMPT is deduced from the existence of extracellular NAMPT (eNAMPT), which is released from cells in extracellular vesicles.<sup>31</sup> Hence, ample precedent exists for differential sequestration of NAM-generating and -consuming enzymes in the various cellular compartments to explain the disparate metabolic fates of exogenous NAM and  $\text{NAD}^+$ -derived NAM. Results from our cell tracer studies with NAMPT activators raised the fascinating possibility that various  $\text{NAD}^+$  booster strategies (NAMPT activator,  $\text{NAD}^+$  precursor, CD38 inhibitor) might be distinguishable with respect to their effect on different subcellular  $\text{NAD}^+$  pools.

Plasma from mice and humans dosed i.v. with  $^2\text{H}_4$ -NAM had higher levels of NAM(M0) in addition to the expected rise of NAM(M4). Elevated plasma levels of NAM(M0) were consistent with findings from a prior study in which rats dosed with 4,6- $\text{d}_2$ -NAM had increased plasma NAM (i.e., NAM(M0)).<sup>24</sup> It was proposed that 4,6- $\text{d}_2$ -NAM dosing resulted in reversible exchange with an endogenous NAM pool and concomitant NAM release into blood. In our  $^2\text{H}_4$ -NAM tracer investigation, elevated plasma NAM(M0) in mice and humans was accompanied by increased plasma MeNAM(M0) and Me6PY(M0). Hence, NAM displaced from this putative compartment by  $^2\text{H}_4$ -NAM appeared to be subject to typical NAM metabolism. This NAM reservoir may be poised for mobilization in response to an emergent need for  $\text{NAD}^+$  or MeNAM. Possible depletion of this NAM

pool by drugs or dietary constituents that displace NAM from this exchangeable compartment might have a profound impact on NAM homeostasis and  $\text{NAD}^+$  biosynthesis.

Mapping the dual metabolic fates of NAM from the alternative sources helps clarify the impact of NAM on fundamental cellular processes involving  $\text{NAD}^+$  and MeNAM. Deepening our knowledge of the dynamic processes governing the pivotal interplay between NAM,  $\text{NAD}^+$ , and MeNAM will spur the development of novel approaches that tap the vast therapeutic potential of this central metabolic regulatory cascade.

#### Limitations of the study

Herein we sought to determine if the metabolic fate of  $^2\text{H}_4$ -NAM in cultured cells and mice was translatable to humans. Our pioneering clinical study involving i.v. infusion of  $^2\text{H}_4$ -NAM established our ability to trace  $\text{NAD}^+$  synthesis/consumption and MeNAM synthesis in humans. A limitation of this clinical study was the small number of subjects ( $n = 4$  each for the low and high  $^2\text{H}_4$ -NAM dose groups). Future studies with more subjects, and a focus on demographic differences (e.g., age) will address this current limitation and begin to unravel how external influences modulate the rates of  $\text{NAD}^+$  synthesis and consumption in humans. Studies with cultured A549 cells revealed that NAMPT activators reprogrammed the metabolic routing of NAM such that NAM liberated from NAD was newly accessible to NNMT action. We hypothesized that this finding reflected the engagement of a different cell compartment for  $\text{NAD}^+$  synthesis and consumption in the presence of NAMPT activators. A limitation related to this matter is lack of evidence that NAMPT activators reprogrammed NAM metabolism *in vivo*

(mice or humans). Another caveat, as mentioned earlier, is that the biomarker for the apparent reprogramming, MeNAM(M3), might arise from NAM(M3) export followed by cellular import and utilization by NNMT, akin to exogenous NAM. Hence, it is possible that reprogramming of the metabolic fate of NAM with a NAMPT activator might not arise from different compartmentalization barriers but instead might reflect increased NAD<sup>+</sup> consumption and NAM(M3) export. More work is needed to exclude this alternative explanation for the increased MeNAM(M3) in the presence of a NAMPT activator.

## STAR★METHODS

Detailed methods are provided in the online version of this paper and include the following:

- **KEY RESOURCES TABLE**
- **RESOURCE AVAILABILITY**
  - Lead contact
  - Materials availability
  - Data and code availability
- **EXPERIMENTAL MODEL AND SUBJECT DETAILS**
  - *In vivo* mouse studies
  - Human studies
- **METHOD DETAILS**
  - Cell culture
  - Metabolite extractions for targeted metabolomics
  - <sup>2</sup>H<sub>4</sub>-NAM quantitation in human plasma
  - Stable isotope tracer analysis
  - *In vitro* <sup>2</sup>H<sub>4</sub>-NAM tracer experiments with isolated human PBMCs
- **QUANTIFICATION AND STATISTICAL ANALYSIS**
  - Data analysis and statistics
- **ADDITIONAL RESOURCES**

## SUPPLEMENTAL INFORMATION

Supplemental information can be found online at <https://doi.org/10.1016/j.celrep.2023.112218>.

## ACKNOWLEDGMENTS

This work was partially funded by a Moffitt AdventHealth Collaboration grant (S.J.G. and G.M.D.). We thank the AdventHealth Metabolomics Core for performing targeted metabolite assays. NAMPT activators were kindly provided by Drs. A. Pinkerton and M. Jackson (Sanford Burnham Prebys). We thank members of the TRI Clinical Research Unit, Pharmacy, Research Laboratory and Research Administration, who helped launch the NADFLUX clinical study. The NADFLUX clinical study was funded by the AdventHealth Generosity Champions Giving Program.

## AUTHOR CONTRIBUTIONS

Conceptualization, S.J.G. and G.M.D.; methodology, T.D. and S.J.G.; investigation, T.D., N.K., M.M., S.C., N.P.-F., A.F., and N.P.W.; clinical study planning, S.J.G., P.M.C., J.P.D., and S.R.S.; writing, S.J.G. and T.D.; supervision, S.J.G., G.M.D., and T.D.

## DECLARATION OF INTERESTS

The authors declare no competing interests.

Received: September 13, 2022

Revised: January 17, 2023

Accepted: February 17, 2023

## REFERENCES

1. Xiao, W., Wang, R.S., Handy, D.E., and Loscalzo, J. (2018). NAD(H) and NADP(H) redox couples and cellular energy metabolism. *Antioxid. Redox Signal.* *28*, 251–272.
2. Covarrubias, A.J., Perrone, R., Grozio, A., and Verdin, E. (2021). NAD(+) metabolism and its roles in cellular processes during ageing. *Nat. Rev. Mol. Cell Biol.* *22*, 119–141.
3. Consortium, G.T. (2013). The genotype-tissue expression (GTEx) project. *Nat. Genet.* *45*, 580–585.
4. Ulanovskaya, O.A., Zuhl, A.M., and Cravatt, B.F. (2013). NNMT promotes epigenetic remodeling in cancer by creating a metabolic methylation sink. *Nat. Chem. Biol.* *9*, 300–306.
5. Kitamura, S., Nitta, K., Tayama, Y., Tanoue, C., Sugihara, K., Inoue, T., Horie, T., and Ohta, S. (2008). Aldehyde oxidase-catalyzed metabolism of N1-methylnicotinamide in vivo and in vitro in chimeric mice with humanized liver. *Drug Metab. Dispos.* *36*, 1202–1205.
6. Hayat, F., Sonavane, M., Makarov, M.V., Trammell, S.A.J., McPherson, P., Gassman, N.R., and Migaud, M.E. (2021). The biochemical pathways of nicotinamide-derived pyridones. *Int. J. Mol. Sci.* *22*, 1145.
7. Pissios, P. (2017). Nicotinamide N-methyltransferase: more than a vitamin B3 clearance enzyme. *Trends Endocrinol. Metab.* *28*, 340–353.
8. Nejabati, H.R., Mihanfar, A., Pezeshkian, M., Fattahi, A., Latifi, Z., Safaie, N., Valiloo, M., Jodati, A.R., and Nouri, M. (2018). N1-methylnicotinamide (MNAM) as a guardian of cardiovascular system. *J. Cell. Physiol.* *233*, 6386–6394.
9. Ström, K., Morales-Alamo, D., Ottosson, F., Edlund, A., Hjort, L., Jörgensen, S.W., Almgren, P., Zhou, Y., Martin-Rincon, M., Ekman, C., et al. (2018). N(1)-methylnicotinamide is a signalling molecule produced in skeletal muscle coordinating energy metabolism. *Sci. Rep.* *8*, 3016.
10. Kannt, A., Pfenninger, A., Teichert, L., Tönjes, A., Dietrich, A., Schön, M.R., Klötting, N., and Blüher, M. (2015). Association of nicotinamide-N-methyltransferase mRNA expression in human adipose tissue and the plasma concentration of its product, 1-methylnicotinamide, with insulin resistance. *Diabetologia* *58*, 799–808.
11. Kilgour, M.K., MacPherson, S., Zacharias, L.G., Ellis, A.E., Sheldon, R.D., Liu, E.Y., Keyes, S., Pauly, B., Carleton, G., Allard, B., et al. (2021). 1-Methylnicotinamide is an immune regulatory metabolite in human ovarian cancer. *Sci. Adv.* *7*, eabe1174.
12. Eckert, M.A., Coscia, F., Chryplewicz, A., Chang, J.W., Hernandez, K.M., Pan, S., Tienda, S.M., Nahotko, D.A., Li, G., Blaženović, I., et al. (2019). Proteomics reveals NNMT as a master metabolic regulator of cancer-associated fibroblasts. *Nature* *569*, 723–728.
13. Lu, S., Ke, S., Wang, C., Xu, Y., Li, Z., Song, K., Bai, M., Zhou, M., Yu, H., Yin, B., et al. (2022). NNMT promotes the progression of intrahepatic cholangiocarcinoma by regulating aerobic glycolysis via the EGFR-STAT3 axis. *Oncogenesis* *11*, 39.
14. Olsson, A., Olofsson, T., and Pero, R.W. (1993). Specific binding and uptake of extracellular nicotinamide in human leukemic K-562 cells. *Biochem. Pharmacol.* *45*, 1191–1200.
15. Suzuki, E., Okuda, H., Nishida, K., Fujimoto, S., and Nagasawa, K. (2010). Protective effect of nicotinamide against poly(ADP-ribose) polymerase-1-mediated astrocyte death depends on its transporter-mediated uptake. *Life Sci.* *86*, 676–682.
16. Gardell, S.J., Hopf, M., Khan, A., Dispagna, M., Hampton Sessions, E., Falter, R., Kapoor, N., Brooks, J., Culver, J., Petucci, C., et al. (2019). Boosting NAD(+) with a small molecule that activates NAMPT. *Nat. Commun.* *10*, 3241.

17. Kannt, A., Rajagopal, S., Kadnur, S.V., Suresh, J., Bhamidipati, R.K., Swaminathan, S., Hallur, M.S., Kristam, R., Elvert, R., Czech, J., et al. (2018). A small molecule inhibitor of nicotinamide N-methyltransferase for the treatment of metabolic disorders. *Sci. Rep.* **8**, 3660.
18. Hara, N., Shibata, T., Osago, H., Yamada, K., and Tsuchiya, M. (2014). Formation of [nicotinamide-(2)H(3)]NAD(+) from [(2)H(4)]nicotinamide and [(2)H(4)]nicotinic acid in human HepG2N cells and involvement of (2)H/(1)H exchange at the redox site of NAD(+)/NADH. *J. Nutr. Sci. Vitaminol.* **60**, 17–21.
19. McReynolds, M.R., Chellappa, K., Chiles, E., Jankowski, C., Shen, Y., Chen, L., Descamps, H.C., Mukherjee, S., Bhat, Y.R., Lingala, S.R., et al. (2021). NAD(+) flux is maintained in aged mice despite lower tissue concentrations. *Cell Syst.* **12**, 1160–1172.e4.
20. Chini, C.C.S., Peclat, T.R., Warner, G.M., Kashyap, S., Espindola-Netto, J.M., de Oliveira, G.C., Gomez, L.S., Hogan, K.A., Tarragó, M.G., Puranik, A.S., et al. (2020). CD38 ecto-enzyme in immune cells is induced during aging and regulates NAD(+) and NMN levels. *Nat. Metab.* **2**, 1284–1304.
21. Ehlerding, E.B., England, C.G., Jiang, D., Graves, S.A., Kang, L., Lacognata, S., Barnhart, T.E., and Cai, W. (2017). CD38 as a PET imaging target in lung cancer. *Mol. Pharm.* **14**, 2400–2406.
22. Tarragó, M.G., Chini, C.C.S., Kanamori, K.S., Warner, G.M., Caride, A., de Oliveira, G.C., Rud, M., Samani, A., Hein, K.Z., Huang, R., et al. (2018). A potent and specific CD38 inhibitor ameliorates age-related metabolic dysfunction by reversing tissue NAD(+) decline. *Cell Metab.* **27**, 1081–1095.e10.
23. Pinkerton, A.B., Sessions, E.H., Hershberger, P., Maloney, P.R., Peddibhotla, S., Hopf, M., Sergienko, E., Ma, C.T., Smith, L.H., Jackson, M.R., et al. (2021). Optimization of a urea-containing series of nicotinamide phosphoribosyltransferase (NAMPT) activators. *Bioorg. Med. Chem. Lett.* **41**, 128007.
24. Linnik, I.V., Rayner, P.J., Stow, R.A., Duckett, S.B., and Cheetham, G.M.T. (2019). Pharmacokinetics of the SABRE agent 4,6-d2-nicotinamide and also nicotinamide in rats following oral and intravenous administration. *Eur. J. Pharm. Sci.* **135**, 32–37.
25. Liu, L., Su, X., Quinn, W.J., 3rd, Hui, S., Krukenberg, K., Frederick, D.W., Redpath, P., Zhan, L., Chellappa, K., White, E., et al. (2018). Quantitative analysis of NAD synthesis-breakdown fluxes. *Cell Metab.* **27**, 1067–1080.e5.
26. Bender, D.A. (1983). Biochemistry of tryptophan in health and disease. *Mol. Aspects Med.* **6**, 101–197.
27. Zeidler, J.D., Chini, C.C.S., Kanamori, K.S., Kashyap, S., Espindola-Netto, J.M., Thompson, K., Warner, G., Cabral, F.S., Peclat, T.R., Gomez, L.S., et al. (2022). Endogenous metabolism in endothelial and immune cells generates most of the tissue vitamin B3 (nicotinamide). *iScience* **25**, 105431.
28. Nikiforov, A., Dölle, C., Niere, M., and Ziegler, M. (2011). Pathways and subcellular compartmentation of NAD biosynthesis in human cells: from entry of extracellular precursors to mitochondrial NAD generation. *J. Biol. Chem.* **286**, 21767–21778.
29. Cambronne, X.A., and Kraus, W.L. (2020). Location, location, location: compartmentalization of NAD(+) synthesis and functions in mammalian cells. *Trends Biochem. Sci.* **45**, 858–873.
30. Svoboda, P., Krizova, E., Sestakova, S., Vapenkova, K., Knejzlik, Z., Rimpelova, S., Rayova, D., Volfova, N., Krizova, I., Rumlova, M., et al. (2019). Nuclear transport of nicotinamide phosphoribosyltransferase is cell cycle-dependent in mammalian cells, and its inhibition slows cell growth. *J. Biol. Chem.* **294**, 8676–8689.
31. Yoshida, M., Satoh, A., Lin, J.B., Mills, K.F., Sasaki, Y., Rensing, N., Wong, M., Apte, R.S., and Imai, S.I. (2019). Extracellular vesicle-contained eN-AMPT delays aging and extends lifespan in mice. *Cell Metab.* **30**, 329–342.e5.
32. Nair, A.B., and Jacob, S. (2016). A simple practice guide for dose conversion between animals and human. *J. Basic Clin. Pharm.* **7**, 27–31.
33. Gonsalves, W.I., Ramakrishnan, V., Hitosugi, T., Ghosh, T., Jevremovic, D., Dutta, T., Sakrikar, D., Petterson, X.M., Wellik, L., Kumar, S.K., and Nair, K.S. (2018). Glutamine-derived 2-hydroxyglutarate is associated with disease progression in plasma cell malignancies. *JCI Insight* **3**, e94543.

## STAR★METHODS

### KEY RESOURCES TABLE

REAGENT or RESOURCE	SOURCE	IDENTIFIER
<b>Antibodies</b>		
Mouse monoclonal anti-NNMT (clone G-4)	Santa Cruz Biotechnology	Sc-376048; AB_10988227
<b>Chemicals, peptides, and recombinant proteins</b>		
SBI-797812 (small molecule NAMPT activator)	Sanford Burnham Prebys Medical Research Institute	Gardell et al. <sup>16</sup>
SBI-801071 (small molecule NAMPT activator)	Sanford Burnham Prebys Medical Research Institute	Pinkerton et al. <sup>23</sup>
NAMPT Inhibitor	Cayman Chemical Company	FK-866
Nicotinamide N-methyltransferase inhibitor (NNMTi)	Cayman Chemical Company	JBSNF-000088
CD38 inhibitor (CD38i)	Calbiochem	Compound 78c
2,4,5,6- <sup>2</sup> H <sub>4</sub> nicotinamide ( <sup>2</sup> H <sub>4</sub> -NAM)	Cambridge Isotope Laboratories	DLM-6883
2,4,5,6- <sup>2</sup> H <sub>4</sub> nicotinamide ( <sup>2</sup> H <sub>4</sub> -NAM) (human study)	CDN Isotopes	D-3457
<sup>13</sup> C <sub>6</sub> -nicotinic acid ( <sup>13</sup> C <sub>6</sub> -NA)	Cambridge Isotope Laboratories	CLM-9954
<sup>13</sup> C <sub>11</sub> -tryptophan ( <sup>13</sup> C <sub>11</sub> -Trp)	Cambridge Isotope Laboratories	CLM-4290
<sup>18</sup> O <sub>2</sub> -β-Nicotinamide adenine dinucleotide	Sanford Burnham Prebys Medical Research Institute	Custom synthesis (see Gardell et al. <sup>16</sup> )
RPMI1640 media (without Gln, glucose, NAM, Trp)	Boca Scientific (Dedham, MA)	Custom product
Nicotinamide (NAM)	Acros Organics	AC128271000
Nicotinamide mononucleotide (NMN)	Sigma Aldrich (St. Louis, MO)	N3501
1-Methyl-6-oxo-1,6-dihydropyridine-3-carboxamide (6-MePY)	Ambeed	A130732
1-Methyl NAM (1-MeNAM)	Fluka	M4627
Nicotinamide adenine dinucleotide (NAD)	Sigma	N1636
Nicotinamide adenine dinucleotide, reduced (NADH)	Sigma	N8129
Perchloric acid (PCA)	Sigma Aldrich (St. Louis, MO)	311421
Acetonitrile (ACN)	Optima	A955-4
Ammonium acetate	Sigma	372331
<b>Critical commercial assays</b>		
Pierce BCA protein assay kit	ThermoFisher Scientific	Cat # 23227
<b>Deposited data</b>		
Raw and analyzed mass spectrometry data	AdventHealth	Upon request
<b>Experimental models: Cell lines</b>		
A549 lung adenocarcinoma cells	ATCC	#CCL-185, RRID: CVCL_0023
<b>Experimental models: Organisms/strains</b>		
NSG Immunodeficient mice for xenograft model	The Jackson Laboratory (Bar Harbor, ME)	NSG (NOD.Cg-Prkdc <sup>scid</sup> Il2rg <sup>tm1Wjl</sup> /SzJ, RRID:IMSR_JAX:005557)

### RESOURCE AVAILABILITY

#### Lead contact

Further information and requests for resources and reagents should be directed to and will be fulfilled by the lead contact, Stephen Gardell, PhD ([stephen.gardell@adventhealth.com](mailto:stephen.gardell@adventhealth.com)).

### Materials availability

This study did not generate new unique reagents.

### Data and code availability

All data reported in this paper will be shared by the [lead contact](#) upon request. This paper does not report original code. Any additional information required to reanalyze the data reported in this paper is available from the [lead contact](#) upon request.

## EXPERIMENTAL MODEL AND SUBJECT DETAILS

### *In vivo* mouse studies

#### *Murine xenograft model and NAD<sup>+</sup> precursor infusion*

Immunodeficient NSG mice (males and females between 87 and 188 days of age) were injected subcutaneously with  $1 \times 10^6$  A549 cells in PBS and allowed to form tumors. Once palpable tumors formed (100–200 mm<sup>3</sup>), labeling with stable isotopes was performed on conscious, unrestrained mice using a jugular catheter to minimize changes in metabolism due to anesthesia. Mice were surgically implanted with a jugular vein cannula at 3–7 days prior to infusion. Mice with jugular vein cannula in place were individually housed. Stable isotope-labeled substrates were infused at a rate of 2  $\mu$ L/min for 240 min using the following infusate concentrations: <sup>13</sup>C<sub>6</sub>-NA, 0.2 mM; <sup>2</sup>H<sub>4</sub>-NAM, 4 mM; <sup>13</sup>C<sub>11</sub>-Trp, 100 mM. All *in vivo* studies were approved by the Moffitt Cancer Center IACUC (protocol #7922).

### Human studies

#### *Dosing human volunteers with <sup>2</sup>H<sub>4</sub>-NAM*

The NADFLUX clinical protocol (PI: S. Gardell) was approved by the AdventHealth-Orlando (Orlando, FL) Institutional Review Board and conducted in agreement with the Declaration of Helsinki. The investigation was fully executed at the AdventHealth Translational Research Institute (TRI) which has the required resources and professional staff including a Medical Oversight Committee and Quality Committee. After obtaining written informed consent, healthy male and female adult participants (N = 2 and 6, respectively) with ages ranging from 22 to 36 years of age (mean = 29.9) and exhibiting BMI values between 22.0 and 29.1 kg/m<sup>2</sup> (mean = 26.5) were enrolled in the study (Table S7). Subjects were admitted to the TRI in a fasting condition at approximately 7:00 A.M. Weight and vital signs were assessed followed by consumption of a standard breakfast. Blood draws (N = 3) were sequentially collected via IV or venipuncture of an antecubital vein in the arm at pre <sup>2</sup>H<sub>4</sub>-NAM infusion (baseline) as well as at 4 hr. and 8 hr. after starting the <sup>2</sup>H<sub>4</sub>-NAM infusion. Blood was drawn into (i) a mononuclear cell preparation tube (sodium citrate); 8 mL blood volume for PBMC isolation and (ii) a BD vacutainer plasma preparation tube (sodium citrate); 4.5 mL blood volume. <sup>2</sup>H<sub>4</sub>-NAM (CDN Isotopes) tested for sterility and pyrogenicity by Applied Research Laboratories and stored as dry powder at the TRI Pharmacy. The TRI Pharmacy staff prepared a stock solution of <sup>2</sup>H<sub>4</sub>-NAM (10 mg mL<sup>-1</sup>) in sterile 0.9% sodium chloride. The stock solution of <sup>2</sup>H<sub>4</sub>-NAM was subsequently diluted to the final infusate concentration in the PID-labeled infusion bag (192 mL) within 24 hr. of the study. <sup>2</sup>H<sub>4</sub>-NAM was administered to participants for 8 hr. via an indwelling peripheral intravenous catheter. The infusion rate used for the first 4 subjects, 0.0031 mg kg<sup>-1</sup> min<sup>-1</sup>, was derived from a human equivalent dose calculation<sup>32</sup> based on a <sup>2</sup>H<sub>4</sub>-NAM infusion study performed with mice.<sup>25</sup> The <sup>2</sup>H<sub>4</sub>-NAM dose received by the final 4 subjects was 0.0062 mg kg<sup>-1</sup> min<sup>-1</sup>. Samples were stored at the TRI with de-identified acoustic codes.

## METHOD DETAILS

### Cell culture

Human A549 lung carcinoma cells were grown in RPMI-1640 media, 11.11 mM D-(+)-glucose, 5% fetal bovine serum (FBS), penicillin/streptomycin mixture in a humidified incubator with 5% CO<sub>2</sub> at 37°C. under standard culture conditions. The A549 cells tested negative for mycoplasma contamination. Standard RPMI-1640 media contained NAM (8.2  $\mu$ M) and Trp (24.5  $\mu$ M) but not nicotinic acid (NA). For certain experiments, custom-synthesized RPMI-1640 media (devoid of NAM, Trp, Gln, and glucose) was used and supplemented with ingredients tailored to the experimental protocol. Cells were grown in 10 cm dishes and routinely treated with NAD<sup>+</sup> precursors and other specified reagents for 18 hr. An exception was the experiment presented in Figure 2 in which cells were grown in 6 well dishes and the contents of 3 wells were combined for each sample. A549 cells were washed with cold PBS containing CD38i (5  $\mu$ M) and covered with liquid nitrogen. After decanting the liquid nitrogen, the frozen cell monolayer was scraped, harvested, and the cell slush was stored at –80°C. Total cellular protein was measured with the BCA Protein assay kit using BSA as the protein standard.

### Metabolite extractions for targeted metabolomics

For assay of oxidized pyridine nucleotides, 10  $\mu$ L of the A549 cell slush was used for protein assay, and 200  $\mu$ L 1 M perchloric acid (PCA) was added to the remaining sample. The samples were vortexed and centrifuged. The supernatant volumes were recorded, and each brought up to 400  $\mu$ L with distilled water. A 100  $\mu$ L aliquot was used for targeted metabolite profiling. A fourteen-point calibration curve (R<sup>2</sup> = 0.99 or greater) was created for each analyte using authentic standard and respective stable isotope labelled internal standard.

### **<sup>2</sup>H<sub>4</sub>-NAM quantitation in human plasma**

<sup>2</sup>H<sub>4</sub>-NAM calibration standards ranging from 0.063 to 32 μM were prepared in water. Plasma samples or standard were mixed with 3X volume of 80% (1:1) MeOH: ACN and 10 μL of <sup>18</sup>O<sub>2</sub>-NAD internal standard (IS). Samples were centrifuged and the supernatants were dried and resuspended in 50 μL 10 mM ammonium acetate (pH 9.5) for analysis by LC-MS/MS. A separate calibration curve for unlabeled NAM, MeNAM and Me6PY was prepared in water with concentrations ranging from 0.01–100 μM using the same metabolite extraction protocol as above to determine the unlabeled (M0) concentrations of NAM, MeNAM and Me6PY in the plasma samples.

### **Stable isotope tracer analysis**

Plasma metabolites were extracted with 80% (1:1) MeOH: ACN and centrifuged at 10,000 × g for 30 min at 4°C. Tissue and PBMC samples were snap-frozen and stored at –80°C. Frozen samples were weighed and homogenized in ice cold 50% MeOH:water (400 μL per 20 mg tissue weight) using a liquid nitrogen-chilled tissue homogenizer (Precellys). Metabolites from A549 cells, PBMCs and tissues were extracted into 80% (1:1) MeOH: ACN + 0.1% formic acid followed by neutralization with 15% (w/v) ammonium bicarbonate and centrifugation at 18,000 × g for 30 min at 4°C. The supernatants were dried and resuspended in 50 μL of 20 mM ammonium bicarbonate (pH 8.0) for analysis using a QExactive Plus Orbitrap MS (QE-MS) with a HESI II probe and coupled with an Ultra High-Pressure Liquid Chromatography (Dionex UltiMate 3000) system. Samples were analyzed within 24 hr. of reconstitution. Reverse-phase (RP) chromatography was performed using HSS C18 column (150 × 2.1 mm i.d., 1.7 mm; Waters) with a flow rate of 0.4 mL/min. Solvent A was 0.1% formic acid in water and solvent B was 0.1% ACN. The LC gradient included a 1 min hold at 0.1% B followed by a ramp from 0.1% to 50% B over the next 7 min followed by a ramp to 99% over the next 8 min. A 3 min hold at 99% was followed by a return to 0% B over the next 0.5 min. The run was completed with a 7 min recondition at 0.1% B. The RP separation was performed over 22 min in positive ionization mode. Nucleotide separation was achieved with BEH amide column (150 × 2.1 mm i.d., 1.7 mm; Waters). The column temperature was set at 30°C and the injection volume was 5 μL. Solvent A is 20 mM ammonium bicarbonate pH 9.5 and solvent B is ACN. The mass spectrometer was operated in positive and negative ESI ion mode in the scan range of m/z 70–1,050 with the resolution of 70,000 at m/z 200, automatic gain control (AGC) target at 1 × 10<sup>6</sup> and maximum injection time of 50 ms. The spray voltage was set to 3.5 and 2.5 kV in positive and negative ion mode, respectively. The heated capillary was set at 200°C; the HESI probe was set at 350°C; and the S-lens RF level was set at 45. The gas settings for sheath, auxiliary and sweep were 40, 10 and 1 unit, respectively. Peak areas (AUC) were used for comparative quantitation.

### **In vitro <sup>2</sup>H<sub>4</sub>-NAM tracer experiments with isolated human PBMCs**

Whole blood (8 mL) was collected into sodium citrate CPT tubes (Becton Dickinson, cat# 362761). PBMCs were isolated according to the CPT tube instructions. The final PBMC pellet was resuspended in DPBS. Live PBMCs cells were counted using trypan blue staining and a countess cell counter. Cells were used immediately for the <sup>2</sup>H<sub>4</sub>-NAM tracer study. PBMCs (2.0 × 10<sup>6</sup> cells) were added to each well of a 6-well culture dish containing 3 mL of RPMI-1640 custom media supplemented with <sup>2</sup>H<sub>4</sub>-NAM and the various tool compounds. After 18 hr. at 37°C, cells and CM were harvested and analyzed for the MID profiles of NMN, NAD<sup>+</sup>, NADH, NADP, NAM and MeNAM as described above.

## **QUANTIFICATION AND STATISTICAL ANALYSIS**

### **Data analysis and statistics**

#### **Targeted metabolomics**

Raw data files were processed using Xcalibur 3.0. Calibration curves ( $R^2 = 0.99$  or greater) were either fitted with a linear or a quadratic curve with a 1/X or 1/X<sup>2</sup> weighting. The calibration curves were obtained as plots of the peak area ratio of the target compounds to an IS versus the target compound concentration.

#### **Stable isotope tracer studies**

RAW data files were processed with Xcalibur Quan software (Thermo Scientific). The identity of each mass metabolite was confirmed with the respective authentic standard and the data was corrected for natural isotopic abundance. An in-house library containing all possible <sup>2</sup>H and <sup>13</sup>C isotopologues (m/z of M0, M1, M2, M3 ... Mn) of each relevant metabolite was used for the assignment of AUC of LC-MS signals. Fractional enrichment for each targeted metabolite is an index of the relative flux as calculated from the MID profile using a linear simultaneous equation.<sup>33</sup> Statistical analysis was performed as described in the text or Materials and Methods using GraphPad Prism 8 or Microsoft Excel. We used unpaired t tests for comparison between two groups or ANOVA for groups more than two, as appropriate. For metabolomic analysis, significance testing ( $p < 0.05$ ) was performed on means of quadruplicate measurements or as otherwise mentioned.

## **ADDITIONAL RESOURCES**

The NADFLUX clinical study was registered at [clinicaltrials.gov](https://clinicaltrials.gov) with identifier [04905446](https://clinicaltrials.gov/ct2/show/study/NCT04905446).